JOURNAL OF GEOPHYSICAL RESEARCH, VOL. 112, D16205, doi:10.1029/2007JD008432, 2007

Aerosols in polar regions: A historical overview based on optical depth and in situ observations

C. Tomasi,[1] V. Vitale,[1] A. Lupi,[1] C. Di Carmine,[1] M. Campanelli,[2] A. Herber,[3] R. Treffeisen,[4] R. S. Stone,[5] E. Andrews,[5] S. Sharma,[6] V. Radionov,[7] W. von Hoyningen-Huene,[8] K. Stebel,[9] G. H. Hansen,[9] C. L. Myhre,[9] C. Wehrli,[10] V. Aaltonen,[11] H. Lihavainen,[11] A. Virkkula,[11] R. Hillamo,[11] J. Ström,[12] C. Toledano,[13] V. E. Cachorro,[13] P. Ortiz,[13] A. M. de Frutos,[13] S. Blindheim,[14] M. Frioud,[14] M. Gausa,[14] T. Zielinski,[15] T. Petelski,[15] and T. Yamanouchi[16]

Received 18 January 2007; revised 23 April 2007; accepted 30 May 2007; published 21 August 2007.

[1] Large sets of filtered actinometer, filtered pyrheliometer and Sun photometer measurements have been carried out over the past 30 years by various groups at different Arctic and Antarctic sites and for different time periods. They were examined to estimate ensemble average, long-term trends of the summer background aerosol optical depth AOD(500 nm) in the polar regions (omitting the data influenced by Arctic haze and volcanic eruptions). The trend for the Arctic was estimated to be between −1.6% and −2.0% per year over 30 years, depending on location. No significant trend was observed for Antarctica. The time patterns of AOD(500 nm) and Ångström's parameters α and β measured with Sun photometers during the last 20 years at various Arctic and Antarctic sites are also presented. They give a measure of the large variations of these parameters due to El Chichon, Pinatubo, and Cerro Hudson volcanic particles, Arctic haze episodes most frequent in winter and spring, and the transport of Asian dust and boreal smokes to the Arctic region. Evidence is also shown of marked differences between the aerosol optical parameters measured at coastal and high-altitude sites in Antarctica. In situ optical and chemical composition parameters of aerosol particles measured at Arctic and Antarctic sites are also examined to achieve more complete information on the multimodal size distribution shape parameters and their radiative properties. A characterization of aerosol radiative parameters is also defined by plotting the daily mean values of α as a function of AOD(500 nm), separately for the two polar regions, allowing the identification of different clusters related to fifteen aerosol classes, for which the spectral values of complex refractive index and single scattering albedo were evaluated.

Citation: Tomasi, C., et al. (2007), Aerosols in polar regions: A historical overview based on optical depth and in situ observations, *J. Geophys. Res.*, *112*, D16205, doi:10.1029/2007JD008432.

1. Introduction

[2] Aerosol particles are known to cause significant effects on the radiative balance of the Earth, both directly, through scattering and absorption of short-wave and long-wave radiation [*Charlson et al.*, 1992], and indirectly, by acting as condensation nuclei. The indirect effect (1) enhances the liquid water content of clouds, (2) favors an increase in cloud duration, and (3) strongly influences the heterogeneous chemistry of the atmosphere [*Schwartz et al.*, 1995].

[1]Institute of Atmospheric Sciences and Climate, Consiglio Nazionale delle Ricerche, Bologna, Italy.
[2]Institute of Atmospheric Sciences and Climate, Consiglio Nazionale delle Ricerche, Rome, Italy.
[3]Alfred Wegener Institute of Polar and Marine Research, Bremerhaven, Germany.
[4]Alfred Wegener Institute of Polar and Marine Research, Potsdam, Germany.
[5]Global Monitoring Division, NOAA, Boulder, Colorado, USA.
[6]Science and Technology Branch, Environment Canada, Toronto, Ontario, Canada.
[7]Arctic and Antarctic Research Institute, St. Petersburg, Russia.
[8]Institute of Environmental Physics/Remote Sensing, University of Bremen, Bremen, Germany.
[9]Polar Environmental Centre, Norwegian Institute for Air Research, Tromsø, Norway.
[10]Physikalisch-Meteorologisches Observatorium/World Radiation Centre, Davos, Switzerland.
[11]Finnish Meteorological Institute, Helsinki, Finland.
[12]Department of Applied Environmental Science, Stockholm University, Stockholm, Sweden.
[13]Grupo de Óptica Atmosférica, Universidad de Valladolid, Valladolid, Spain.
[14]Andoya Rocket Range, Andenes, Norway.
[15]Institute of Oceanology, Polish Academy of Sciences, Sopot, Poland.
[16]National Institute of Polar Research, Tokyo, Japan.

0148-0227/07/2007JD008432$09.00

In Polar regions, where the surface albedo can exceed 0.85 in areas covered by snow and ice, aerosols may produce appreciable warming at the surface, if highly absorbing particles are suspended above these bright surfaces due to multiple reflection [*Chylek and Coakley*, 1974; *Randles et al.*, 2004]. While such effects are due mainly to the direct scattering and absorption of incoming solar radiation, exchanges of thermal radiation between the surface and atmosphere enhance heating below dense aerosol layers. It is important to determine the radiative properties of particles within the entire atmospheric column to evaluate accurately the radiative forcing induced by the mixture, both at the top (TOA) and bottom (BOA) of the atmosphere [*Russell et al.*, 1999; *Bush and Valero*, 2002].

[3] To provide valid simulations of TOA and BOA forcing, it is essential to define the aerosol optical and physical parameters (spectral aerosol optical depth (AOD), size distribution, single scattering albedo, asymmetry factor and phase function) and also the spectral and angular dependence of surface reflectance. Improving our knowledge of polar aerosols and their radiative impacts is important in order to arrive at a more realistic evaluation of changes in the Earth's radiative balance, especially in an age when polar albedo is decreasing because of reductions in sea ice and snow cover [e.g., *de la Mare*, 1997; *Robinson*, 1997; *Vinnikov et al.*, 1999; *Hu et al.*, 2004; *Serreze et al.*, 2003; *Holland et al.*, 2006].

[4] To address topics related to the radiative forcing by Polar aerosols in particular, a program referred to as POLAR-AOD has been approved as a major (''cluster'') project to be undertaken during the International Polar Year (IPY). This project has been designated # 171 and is planned over the period from March 2007 to February 2009 (see IPY web page, http://www.ipy.org/development/eoi/proposal-details.php?id=171). The primary goal of this effort is to define ''the means, variability, and trends of the climate-forcing properties of aerosols in polar regions.'' Activities will involve numerous cooperative institutes, including 40 research groups from 22 countries. The most specific tasks will include the following: (1) perform regular measurements of AOD, Ångström's turbidity parameters α and β, and other radiative parameters (Sun photometer intercalibration campaigns and adoption of common protocols to process field data); (2) improve in situ optical and chemical measurements to augment the knowledge on the radiative properties of columnar aerosols; (3) characterize the polar aerosol of different origins, in terms of size distribution, composition and radiative behavior; and (4) establish a data archive of spectral Sun photometer measurements, in situ measurements and derived radiative parameters of aerosols observed in the Polar atmosphere.

[5] Such activities will expand the network and complement the activities already underway under the Global Atmosphere Watch (GAW) program. In support of these tasks, 14 research groups, now working in the context of a POLAR-AOD IPY network, have contributed results from their historic and ongoing measurements of aerosol radiative properties (e.g., spectral AOD, α and β). Some of the groups have been performing measurements at Arctic and Antarctic sites for over 30 years, having a long-standing experience in using multiple wavelength solar radiometers. Equipped with low drift combinations of well blocked interference filters and stable and reliable solid state detectors, these instruments have provided data which were examined following the Sun photometry criteria and the operational procedures defined by *Shaw et al.* [1973]. The groups are listed in Table 1, together with the main spectral characteristics of the radiometers employed (filtered pyrheliometers, actinometers, Sun photometers, Sun and sky radiometers, and star radiometers) and the stations where the instruments are located. Describing the most significant results found by the POLAR-AOD groups during the last decades is the primary focus of this paper. Complementary in situ measurements by other entities listed in Table 2 are included to show their consistency with the AOD measurements, and to give an idea of how an overall picture of the radiative, microphysical and chemical parameters of polar aerosols can be developed. Such analyses are useful when evaluating radiative forcing by aerosols and are needed to reduce uncertainties in climate predictions. Measurements and analysis for the Arctic are given in section 2, and for the Antarctic sites in section 3. Section 4 presents a summary of the polar region aerosol and, in particular, reveals how there is a systematic relationship between the Ångström exponent α and AOD which may form the basis of a parameterization of aerosols for climate studies.

2. Arctic Aerosols

2.1. Arctic Aerosol Optical Depth AOD: Seasonality and Long-Term Trends

[6] Long-term measurements of atmospheric turbidity were performed from 1977 to 1991 at the stations of Severnaya Zemlya, Dikson Island, Kotel'ny Island, and Wrangel Island, all situated along the Siberian coast of the Arctic Ocean, and at Vaida Bay on the Barents Sea coast. The measurements were carried out using thermoelectric actinometers equipped with a set of glass bandpass filters, having short-wavelength cutoffs at 0.38, 0.47, 0.53, 0.63. and 0.71 μm. Monthly mean values of aerosol optical depth AOD at the 500 nm wavelength, and Ångström's parameters α and β were derived from these actinometric measurements [*Radionov and Marshunova*, 1992; *Radionov et al.*, 1994; *Radionov*, 2005]. The interannual variability of the monthly mean AOD at Severnaya Zemlya, Dikson Island and Kotel'ny Island for 1981–1991 is shown in Figure 1. The results clearly indicate that AOD(500 nm) is considerably higher during late winter and spring than in summer, ranging between about 0.10 and 0.30 and between 0.05 and 0.15, respectively. The enhanced turbidity from January to May results from episodes of Arctic haze.

[7] The time series of monthly mean values of AOD(500 nm) for the Siberian stations are again shown in Figure 2 for comparison with two other time series, one from Barrow, Alaska, and the other from Ny Ålesund, Spitsbergen in the Svalbard Archipelago (Norway). Assuming only the summer months, July to September, which present clean air background conditions, and discarding the data relative to the 1982–1984 and 1992–1994 periods, during which the AOD measurements were strongly affected by stratospheric particle extinction due to the El Chichon and Pinatubo volcanic eruptions, respectively [*Stone et al.*, 1993], these segments were fitted linearly to examine trends for the Siberian stations, Barrow and Ny Ålesund.

Table 1. List of the Research Groups Working at Arctic and Antarctic Stations, With the Instruments Used to Perform the Spectral Measurements of AOD and the Main Aerosol Radiative Parameters

Research Group	Sun Photometers, Sun and Sky Radiometers, Star Photometers	Spectral Range, nm	Number of Spectral Channels	Arctic and Antarctic Stations and Activity Periods
ISAC-CNR (Italy)	UVISIR-2 [*De Santis et al.*, 1994], FISBAT [*Tomasi et al.*, 1983], ASP-15WL [*Tomasi et al.*, 2000], PREDE POM 01L [*Di Carmine et al.*, 2005]	320–1047, 400–1041, 321–1026, 315–1020	12, 8, 15, 6	Terra Nova Bay "Mario Zucchelli station" (74°42′S, 164°07′E, 15 MSL), since 1988
AWI (Germany)	SP1A [*Herber et al.*, 2002], SP2H [*Herber et al.*, 2002], STAR01 [*Herber et al.*, 2002]	351–1062, 367–1045, 390–1050	17, 14, 10	Ny Ålesund "AWIPEV station" (78°54′N, 11°53′E, 2 MSL), since 1991; Neumayer (70°38′S, 8°15′W, 40 MSL), since 1991; and Kohnen (75°00′S, 00°04′E, 2892 MSL), since 1991
GMD/NOAA (USA)	SP01-A [*Stone*, 2002], SP01-A, SP02 [*Dutton et al.*, 2004], SP02, ISAC-NOAA	367–865, 413–865, 412–862, 368–1050, 368–1050	4, 4, 4, 8, 8	Barrow (71°19′N, 156°36′W, 8 MSL) in 2000, and South Pole (90°00′S, 139°16′E, 2841 MSL) in 1999/2000; Barrow in 2002–2005, and South Pole in 2000/2001; Barrow in 2001–2002, and South Pole since 2001; Barrow since 2006, and Alert (82°28′N, 62°30′W, 210 MSL), since 2004; Dome C (75°06′S, 123°21′E, 3233 MSL), in January 2003 and since 2005/2006
AARI (Russia)	filtered actinometer M-3 and Sun photometers [*Radionov and Marshunova*, 1992; *Radionov*, 2005].	380–4000, 395–1040	5, 8	Dikson Island (76°30′N, 87°54′E), Severnaya Zemlya (79°00′N, 100°00′E), Kotel'ny Island (76°00′N, 137°54′E), Vaida Bay (69°56′N, 32°00′E) and Wrangel Island (71°14′N, 179°36′W), from 1981 to 1991; Mirny (66°33′S, 93°01′E, 40 MSL), since 1979; and Molodezhnaya (67°40′S, 45°50′E, 42 m MSL) in 1984, 1986, and 1988
PMOD/WRC (Switzerland)	PFR (Precision Filter Radiometer) [*Wehrli*, 2005]	368–862	4	Summit (72°20′N, 38°45′W, 3270 MSL), since 2001
FMI (Finland)	PFR (N29 and N32) [*Wehrli*, 2005], Microtops II (Solar Light web page, http://www.solar.com/sunphoto.htm)	368–862, 380–870	4, 5	Sodankylä (67°22′N, 26°38′E, 184 MSL), since summer 2004; Marambio (64°14′S, 56°37′W, 205 MSL), since 2005; Aboa (73°03′S, 13°25′W, 400 MSL), in January 2000 only
NILU (Norway)	PFR (N18) [*Wehrli*, 2005]	368–862	4	Ny Ålesund Sverdrup station (78°58′N, 11°54′E, 474 MSL), since April 2002; Troll (72°00′S, 2°32′E, 1298 MSL), planned from 2007
GOA - Valladolid Univ. (UVA) (Spain), Andoya Rocket Range (Norway) and NILU (Norway)	CIMEL CE-318-1 [*Holben et al.*, 1998]	440–1020	5	ALOMAR (69°17′N, 16°00′E, 380 MSL), Andenes (Norway), since 2002
Institute of Oceanology, PAS (Poland)	Microtops II (Solar Light web page, http://www.solar.com/sunphoto.htm)	380–870	5	Hornsund (77°00′N, 15°33′E, 10 MSL) in the Svalbard Islands, and aboard the vessel OCEANIA in the Greenland Sea, since 2001
Japan Meteorological Agency (Japan)	EKO MS-110 and MS-120S [*Ohno*, 2005]	368–862	5	Syowa (69°00′S, 39°35′E, 29 MSL), since 1985
National Institute of Polar Research (NIPR), (Japan)	Prede POM-01 and POM-02 sky-radiometers [*Aoki and Fujiyoshi*, 2003]	315–1020	7	Ny Ålesund Rabben station (78°54′N, 11°53′E, 12 MSL), since March 2000; Syowa (69°00′S, 39°35′E, 29 MSL), since January 2001

Table 2. List of the Research Groups Performing the in Situ Measurements Discussed in the Present Paper, at Various Sites and Using Different Instrumental Setups

Research Group	Arctic and Antarctic Stations	Instruments
NOAA/GMD (USA)	Barrow (71°19′N, 156°36′W, 8 MSL)	MRI nephelometer (1976–1998), TSI nephelometer (1997–present), Aethalometer (1988–1999), PSAP (1997–present), CN counter (1976–present)
NOAA/GMD (USA)	South Pole (90°00′S, 139°16′E, 2841 m MSL)	MRI nephelometer (1979–2002), TSI nephelometer (2002–present), Aethalometer (1987–1990), CN counter (1974–present)
NOAA/PMEL (USA)	Barrow (71°19′N, 156°36′W, 8 MSL)	chemical filters
Environment Canada (Canada)	Alert (82°28′N, 62°30′W, 210 MSL)	Nephelometer, PSAP, Aethalometer
MISU (Un. Stockholm)/NILU (Sweden and Norway)	Zeppelin (78°58′N, 11°54′E, 474 MSL)	DMPS, OPC, Nephelometer
FMI (Finland)	GAW Pallas (67°58′N, 24°07′E, 560 MSL)	DMPS, CPC (TSI model) counters, Nephelometer
FMI (Finland)	Aboa (73°03′S, 13°25′W, 400 MSL)	SDI low pressure impactor, VI and ILVS impactors, DMPS, LPC and CPC (TSI model) counters, Nephelometer, Aethalometer
IIA-CNR/FMI (Italy and Finland)	Terra Nova Bay (74° 42′S, 164° 07′E, 15 MSL)	Berner low pressure impactors, Denuders
AWI (Germany)	Neumayer (70°38′S, 8°15′W, 40 MSL), Kohnen (75°00′S, 00°04′E, 2892 MSL)	high-volume and low-volume aerosol sampling systems, CN counters, Aethalometer at both sites

[8] The first set of Siberian data shows that AOD(500 nm) was subject to decrease with an average trend of about −7.6% per year, over the period from 1981 to 1991, presumably as a result of the sharply diminishing anthropogenic emissions of SO_2 from Europe and Russia, especially after 1985. The analysis of the Barrow summer values of AOD_{eff} [*Dutton and Christy*, 1992] yielded an average trend of −1.6% per year over the 25-year period from 1977 to 2002, while the regression line obtained for the AWI data set was found to have an average slope coefficient of −2.2% per year, over the period from 1991 to 2006. The results offer evidence of a long-term decreasing trend of the background values of AOD measured for cloudless background conditions (i.e., unperturbed by volcanic events, Arctic haze occurrence or forest fire episodes), which can be estimated to be approximately within −1.6% and −2.0% per year over the last 30 years, as a consequence of the gradually diminishing emissions of pollutants in the continental areas.

[9] In order to check the reliability of these results, it was decided to analyze the series of monthly average values of the volume scattering coefficient σ_s(550 nm) downloaded from the NOAA/GMD archive (see Barrow archive web page, ftp://ftp.cmdl.noaa.gov/aerosol/brw/archive/), determined through nephelometer measurements performed at Barrow over the period 1976–2005. Analyzing the overall data set relative to the summer months, the regression line was found to have a positive slope coefficient, equal to +1.5% per year. However, considering only the values of $\sigma_s(550\ \text{nm}) \leq 2\ \text{Mm}^{-1}$, pertaining to the best transparency conditions of the atmosphere (background aerosols) and, hence, not including enhanced extinction effects due to optically dense aerosols and boreal smoke particles, a negative slope coefficient was determined, equal to −1.0% per year, which satisfactorily agrees with the negative trends obtained in Figure 2.

[10] The "long-term" measurements presented in Figure 2 show very clearly that a strong AOD contribution was given by the volcanic particles generated by the El Chichon and Pinatubo eruptions in 1982 and 1991, respectively, followed by evident decay features in the subsequent 2–3 years [e.g., *Stone et al.*, 1993], eventually vanishing as a result of dispersion by atmospheric winds and removal by scavenging/precipitation. In addition, Figure 2 shows that AOD(500 nm) assumes rather high values varying mainly between 0.12 and 0.25 during the winter and spring months, as a result of the numerous Arctic haze episodes, which are comparable to those usually measured at midlatitude stations of the continental areas in the Northern Hemisphere. In fact, these episodes are often associated with the intense transport of pollutants from the midlatitudes to the high latitudes, occurring in a seasonal period in which the atmosphere cleaning due to the scavenging of particles by precipitations is particularly weak.

[11] In addition to the historic Siberian actinometric measurements of the atmospheric turbidity parameters, more precise spectral measurements of AOD have been made by some of the groups listed in Table 1. The daily

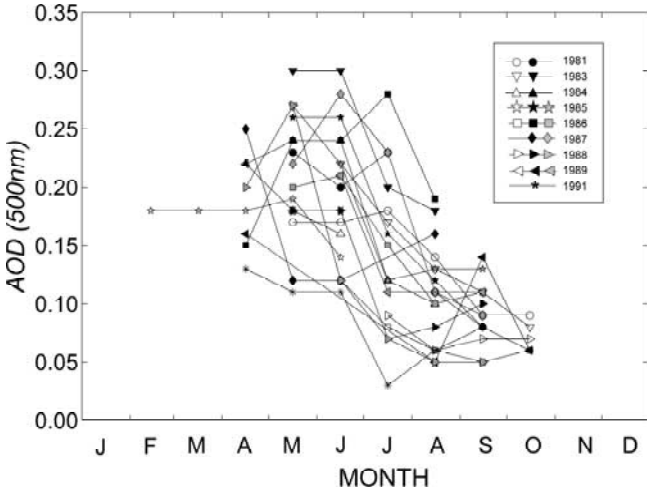

Figure 1. Annual cycles of the monthly mean values of AOD(500 nm) measured at the Siberian stations of Severnaya Zemlya (open symbols), Dikson Island (solid symbols) and Kotel'ny Island (shaded symbols) during the period from 1981 to 1991.

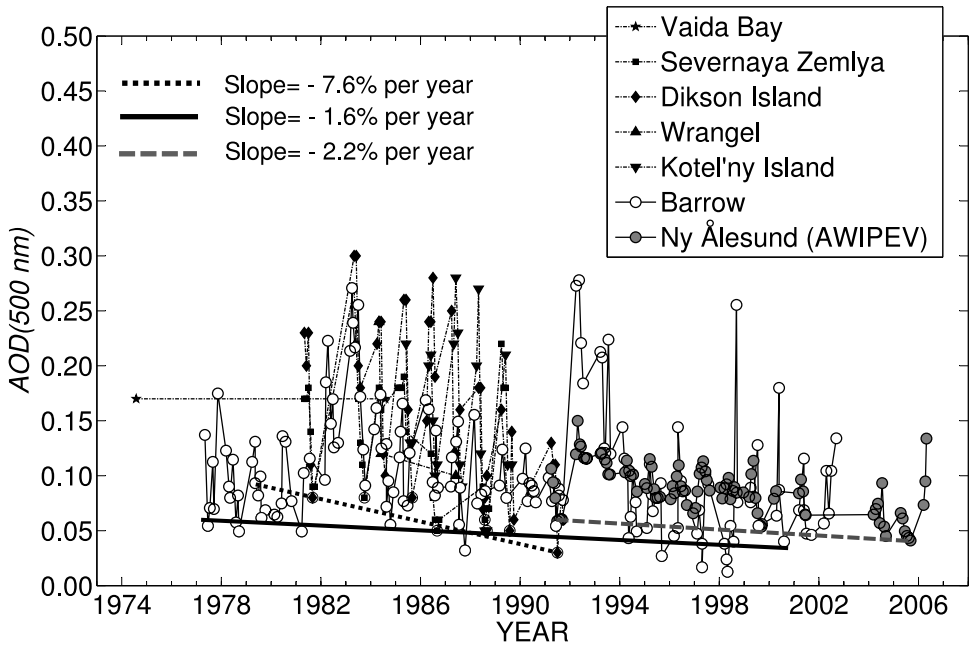

Figure 2. Time patterns of the monthly mean values of AOD(500 nm) measured at different Arctic sites from 1974 to 2006: Siberian data (solid symbols); Barrow measurements of AOD_{eff} (open circles), as derived from filtered pyrheliometer measurements; and Ny Ålesund (AWIPEV) data (shaded circles), derived from Sun photometer measurements. The regression lines were drawn to fit the data relative to the summer months (without volcanic data), assumed as AOD background values: dotted line refers to the overall Siberian data set, solid line refers to the Barrow data set, and grey dashed line refers to the AWIPEV data set.

mean values of AOD(500 nm) measured at the Arctic stations of Barrow (Alaska), Alert (Canada), Summit (Greenland), Ny Ålesund (AWIPEV and NILU stations), Hornsund in the Spitsbergen, ALOMAR in Norway, and Sodankylä in Finland are presented in Figure 3, for various periods between 1991 and 2006. The time series from Ny Ålesund clearly show the incursion and subsequent decay of the Pinatubo aerosol after the 1991 eruptions. More recent composite plots define the periods of enhanced turbidity in late winter and spring, resulting from Arctic haze occurrence. These features agree closely with the seasonal trends of AOD(500 nm) determined by *Shaw* [1982] at Barrow and Fairbanks, in Alaska. Springtime peaks sometimes overlap or are caused by the arrival of dust plumes from Asian deserts and, in late spring and summer, by smoke from fires that burn millions of hectares of boreal forest each year across North America and Siberia. Such events are discussed in section 2.4.

2.2. Covariance of AOD and Ångström Parameters in the Arctic

[12] The spectral series of AOD measured each day at the above eight stations were examined to derive the corresponding values of atmospheric turbidity parameters α and β, following the best fit procedure based on the well-known *Ångström* [1964] formula, which represents the spectral values of AOD as products of β by the inverse power of wavelength λ (measured in μm) with exponent α. This parameter defines the average slope of the spectral dependence curve of AOD and, therefore, its high values indicate the optical predominance of the fine particles over those of larger sizes (i.e., large accumulation and coarse particles), while low values of α indicate the opposite behavior. Parameter β is in practice an average estimate of AOD at unit wavelength and can be used to evaluate the amount of aerosols suspended in the vertical atmospheric column, revealing in some cases the presence of thin clouds

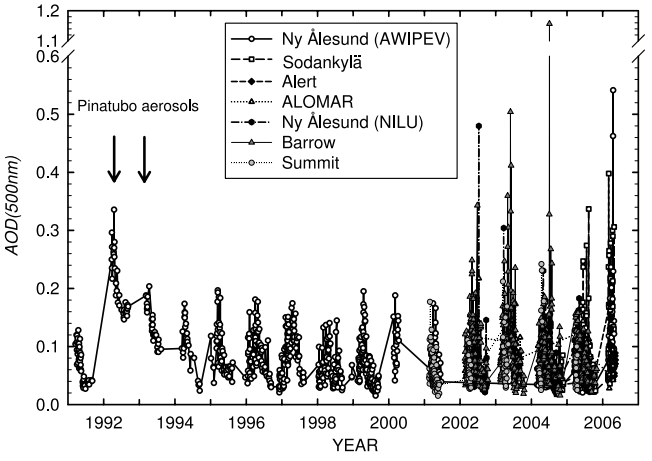

Figure 3. Time patterns of the daily mean values of AOD(500 nm) measured at seven Arctic stations from 1991 to 2006, showing the peaks due to the presence of Pinatubo volcanic particle loadings from 1992 to 1994 and those associated with the Arctic haze episodes frequently observed in the subsequent years, mainly in late winter and early spring.

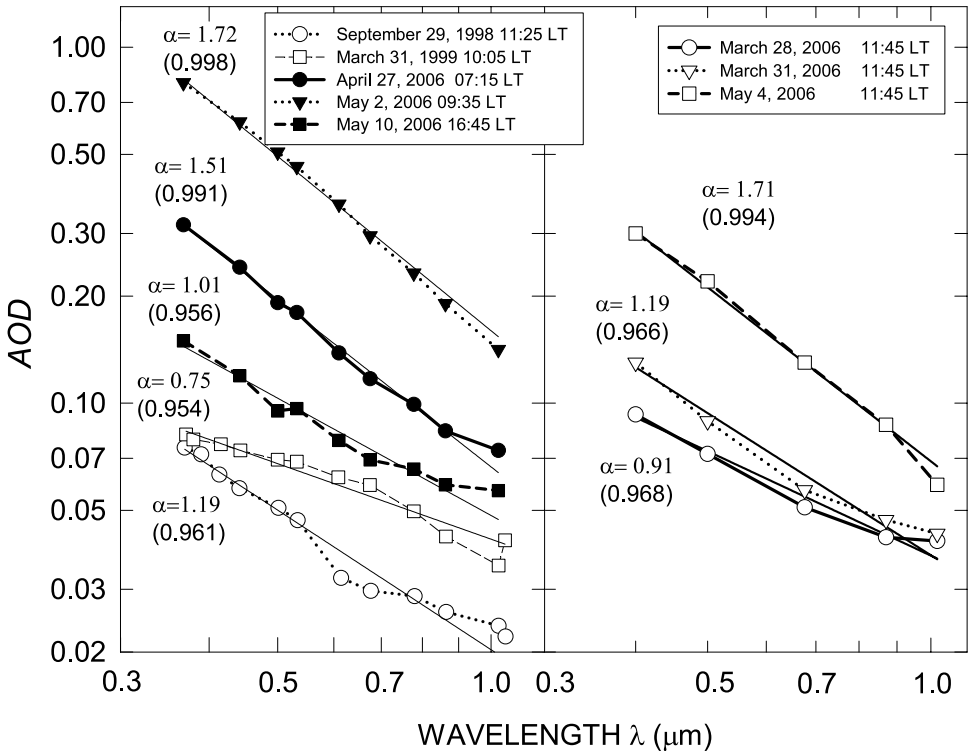

Figure 4. (left) Examples of the *Ångström* [1964] best fit procedure applied to five AOD spectral series measured at the Ny Ålesund (Koldewey/AWIPEV) station, using the SP1A and SP2H Sun photometers [*Herber et al.*, 2002] on clean air days (open symbols) and during the intense Arctic haze transport episode from late April to early May 2006 (solid symbols). (right) As in Figure 4 (left) for three AOD spectral series measured at the Ny Ålesund (Rabben/NIPR) station, using the Prede POM-02 sky radiometer [*Shiobara et al.*, 2006]. The best fit values of exponent α are given for all the best fit lines, together with the corresponding regression coefficients (in brackets).

along the Sun path. Some examples of the Ångström best fit procedure are shown in Figure 4, for spectral series of AOD measured at the Koldewey (AWIPEV) and Rabben (NIPR) stations (Ny Ålesund), which offer the opportunity of verifying that the accuracy of these AOD measurements is of 0.01 in both cases and within all the wavelength channels. Two spectral series of AOD were measured at the Koldewey station for clean air conditions, yielding values of α equal to 1.19 and 0.75, and two other at Rabben in late March 2006, in the absence of haze, presenting values of α equal to 0.91 and 1.19, respectively. Three spectral series of AOD measured at Koldewey and that recorded on 4 May 2006 at Rabben, were taken during the unusual episode of Arctic haze occurring in late April and early May of 2006 [*Shiobara et al.*, 2006]. These measurements are examples of the large increase in AOD caused by the arrival of air masses from Europe, without appreciable changes in the wavelength dependence features of the aerosol extinction along the vertical path. This exceptional Arctic haze episode is examined more carefully in subsection 2.4.3.

[13] At sites where measurements of AOD were taken at fewer wavelengths, parameter α was estimated in terms of a simple pair of AOD values, one taken at a visible wavelength ($\lambda \sim 412$ nm) and the other in the near-IR ($\lambda \sim 675$ nm). The range of values for α will depend on the wavelengths used [*Hand et al.*, 2004] and also on the shape of the size distribution, which may have multiple modes [*Stone*, 2000]. Therefore any comparison of α derived by different methods and/or for different wavelengths must be viewed with caution.

[14] From the daily sets of AOD(500 nm), α and β measured at each station, the daily mean values of the three parameters were calculated at the eight Arctic stations, for the period from 1994 to 2006, and are presented in Figures 5 and 6 The figures omit the data recorded during the transport episodes of Asian dust and Boreal smoke particles, which will be described later. Eight multiannual sets of Sun photometer measurements were considered, carried out using the instruments listed in Table 1 at the following sites: (1) Barrow, from 2002 to 2005; (2) Alert, from 2004 to 2006; (3) Summit, from 2001 to 2005; (4) Ny Alesund (AWIPEV station), from 1994 to 2006 [*Nagel et al.*, 1998; *Herber et al.*, 2002]; (5) Ny Alesund (NILU Sverdrup station), from 2002 to 2006 [*Myhre et al.*, 2006]; (6) Hornsund (Polish Academy of Sciences (PAS)) in the Svalbard region and aboard the IOPAS Oceania vessel, from 2001 to 2003 and in 2006; (7) Sodankylä (FMI station) in the northern Finland, from 2004 to 2006 [*Aaltonen et al.*, 2006a]; and (8) ALOMAR (Andoya Rocket Range) in northern Norway, from 2002 to 2006 [*Toledano et al.*, 2006].

[15] In general, the seasonality of AOD shown in Figures 5 and 6 is similar to that presented previously for the Siberian stations, i.e., higher values of AOD during the

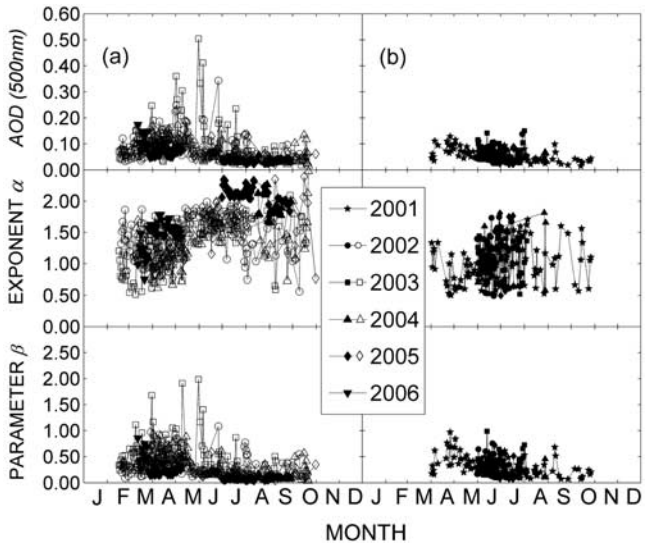

Figure 5. Annual cycles of the daily mean values of AOD(500 nm), Ångström exponent α and parameter β, measured for clear-sky conditions at the Barrow, Alert and Summit sites (where the scale of parameter β is given with values multiplied erroneously by 10). (a) Barrow measurements performed in the 4 years from 2002 to 2005 (open symbols) and the Alert measurements performed in the 3 years from 2004 to 2006 (solid symbols). (b) Summit measurements performed from 2001 to 2005.

Arctic haze season and lower values during summer months. The data sets presented in Figures 5 and 6 show that AOD(500 nm) assumes daily mean values varying between 0.12 and 0.30 in the presence of Arctic haze. Such high AOD values are very close to those observed in the most densely populated and polluted areas of Europe and Northern America. Summer background values of AOD tend to be less than 0.1 and are often less than 0.05. The Ångström parameters also show a seasonal pattern with α being lower during late winter through spring and higher during the summer, while β has the opposite pattern and tends to be in general positively correlated with AOD. Parameter α is sometimes subject to abrupt decreases to values appreciably lower than 1.0. This occurs when there are significant loads of coarse particles with diameters $D >$ 1 μm, and/or when accumulation mode particles of relatively large sizes are suspended above the observation sites. These low values of α are especially noticeable in the Asian dust episodes described in subsection 2.4.1. In other cases, where values of α lower than 0.5 or having negative sign are associated with values of β comparable to those of AOD(500 nm), the AOD data are probably given by the sum of two terms due to background aerosols and thin cirrus clouds, respectively.

[16] Again, caution must be applied in interpreting the value of α, because this parameter provides valid information relating to particle size only in cases where the particle number density decreases with a constant slope as a function of the particle size, according to the *Junge* [1963] model. In such cases, the values of α derived by a single fit over the entire spectral range of the Sun photometer observation can be confidently used to derive the shape of the columnar aerosol size distribution curve. In the many instances, however, as with the occurrence of Arctic haze, Asian dust, aged volcanic aerosols or boreal smoke, the column aerosol size distributions are characterized by bimodal or multimodal features. The retrieval of columnar particle size distributions from spectral series of AOD (using inversion techniques like the one proposed by *King* [1982]), for different values of α ranging between 0.9 and 1.7, suggests that the multimodal size distribution curve of columnar aerosols very often consists of at least two accumulation particle modes centered in the submicron aerosol range, and sometimes of a pronounced coarse particle mode [*Stone*, 2000]. For example, using inversion techniques, *Dutton et al.* [2004] showed that the Arctic haze size spectra inferred from the spectral AOD measurements made at Barrow tend to exhibit bimodal features with an accumulation mode centered at diameter $D_p < 0.4$ μm and a mode centered at $D_p \approx 1.4$ μm, consisting mostly of coarse particles.

2.3. In Situ Measurements of Arctic Haze and Summer Aerosol at the Surface Level

[17] Arctic haze has long been a subject of considerable interest and concern [*Shaw*, 1982, 1983; *Barrie*, 1986], since its source was initially uncertain and attributed to natural factors, such as ice crystals, windblown dust from riverbeds, and Asian dust transport, as supposed by *Rahn et al.* [1977] in studying the haze episode occurring at Barrow in spring 1976. The phenomenon is observed every winter/spring in Alaska, as a consequence of long-range transport [*Harris and Kahl*, 1994]. *Bodhaine and Dutton* [1993] reported a decreasing trend in Arctic haze at Barrow, attributing it to diminished emissions of pollutants in Eurasia after the demise of the Soviet Union. The results of *Rahn et al.* [1977] demonstrated that polluted air masses can be episodically transported in spring from China over the Arctic regions. Thus, considering that the aerosol emissions are presently becoming more intense in such Asian area, it is reasonable to expect a consequent increase in the Arctic haze occurrence within a few years due to these anthropogenic sources. However, a definitive explanation for the trend has not been determined. While emission rates are certain to influence the distribution of haze, changes in atmospheric transport may also be a factor, as suggested by *Jaffe et al.* [1995]. In fact, atmospheric circulation in this region has undergone significant shifts in recent decades, which have resulted in increased cloudiness and warmer temperatures, but diminished snowfall [*Stone*, 1997; *Stone et al.*, 2002].

[18] Historic series of various in situ aerosol properties (i.e., spectral volume scattering coefficient σ_s, spectral volume absorption coefficient σ_a, and particle number concentration N) have been measured at Barrow since the mid-1970s [*Bodhaine*, 1989; *Delene and Ogren*, 2002]. From these direct measurements, radiatively important parameters such as single scattering albedo ω_o, asymmetry parameter and exponent α can be derived. In situ measurements were subsequently taken in the Arctic by other groups using the instruments listed in Table 2. Multichannel nephelometer measurements of in situ coefficient σ_s and exponent α derived from these scattering measurements, are easily compared to the values of AOD and α measured

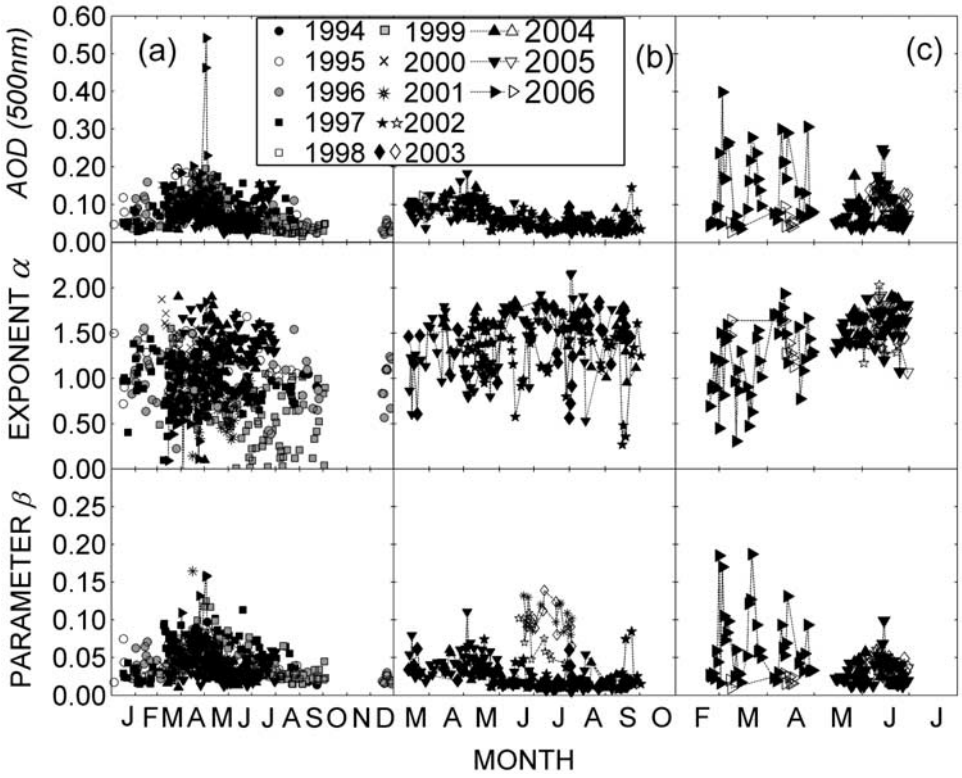

Figure 6. Annual cycles of the daily mean values of AOD(500 nm), Ångström exponent α and parameter β, measured for clear-sky conditions at the Ny Ålesund and Hornsund sites. (a) Ny Ålesund measurements performed by the AWI group during eleven field campaigns from 1994 to 2006. (b) Ny Ålesund measurements performed by the NILU group during four field campaigns from 2002 to 2005 (solid symbols), together with those performed by the IOPAS group at Hornsund and in the Greenland Sea, from 2001 to 2003 and in 2006 (open symbols). (c) Measurements performed by the FMI group at Sodankylä (solid symbols) during three campaigns from 2004 to 2006 and those performed at ALOMAR by the GOA and Andoya Rocket Range groups (open symbols) in four field campaigns from 2002 to 2006.

along the vertical path of the atmosphere. The presence of Arctic haze is often observed in the Barrow aerosol scattering coefficient record [e.g., *Delene and Ogren*, 2002; *Quinn et al.*, 2002]. The annual record of the volume scattering coefficient σ_s for visible light shows similar seasonality to that of AOD observed at Barrow (see Barrow archive web page, ftp://ftp.cmdl.noaa.gov/aerosol/brw/archive/). In fact, it was observed to present both a wide maximum from December to April (Arctic haze period), with the highest monthly median of $\sim$14 Mm^{-1} in January, and a large minimum in June–October, with values of less than 2 Mm^{-1} in June and July, as can be seen in Figure 7 [*Delene and Ogren*, 2002].

[19] The in situ Ångström exponent calculated for the 550 nm/700 nm wavelength pair was found to range between 0.5 (most frequently in August–September) and more than 2 (in May–June) with moderate values in spring, as shown in Figure 7. The overall annual cycle is similar to that derived from AOD measurements (Figure 5a). Typical values of in situ α were found to be around 1.5 during the Arctic haze season [*Delene and Ogren*, 2002]. Evaluations of the monthly median values of ω_o for the visible light were found by *Bodhaine* [1995] to describe an annual cycle with a minimum of $\sim$0.93 in the period of higher Arctic haze occurrence (including late winter and early spring) and more than 0.97 in the summer, from July to September.

[20] Annual mean values of aerosol optical properties were also estimated by *Delene and Ogren* [2002] at Barrow, separately for (accumulation) particles with diameter $D < 1$ μm, and (coarse) particles with diameter $D < 10$ μm, finding (1) $\sigma_s = 6.17 \pm 3.61$ Mm^{-1}, $\sigma_a = 0.36 \pm 0.38$ Mm^{-1}, $\alpha = 1.67 \pm 0.36$, and $\omega_o = 0.954 \pm 0.028$, for the accumulation particles, and (2) $\sigma_s = 9.76 \pm 5.20$ Mm^{-1}, $\sigma_a = 0.39 \pm 0.41$ Mm^{-1}, $\alpha = 1.11 \pm 0.39$, and $\omega_o = 0.965 \pm 0.023$, for the coarse particles.

[21] Recent efforts have focused on correlating the chemical and physical properties of polar aerosols with atmospheric cycles of specific chemical species [*Quinn et al.*, 2002, 2007]. Analyzing a 3-year set of simultaneous measurements of aerosol chemical composition and light scattering and absorption from Barrow, *Quinn et al.* [2002] found sea salt and sulfate aerosol to be the dominant ionic species. The seasonal variations of the concentrations of these two species correlated with the changes in the observed submicron light scattering. Sulfate aerosol dominates submicron scattering during the springtime Arctic haze season, while sea salt is the most important component of submicron scattering in the winter due to wind-driven sea

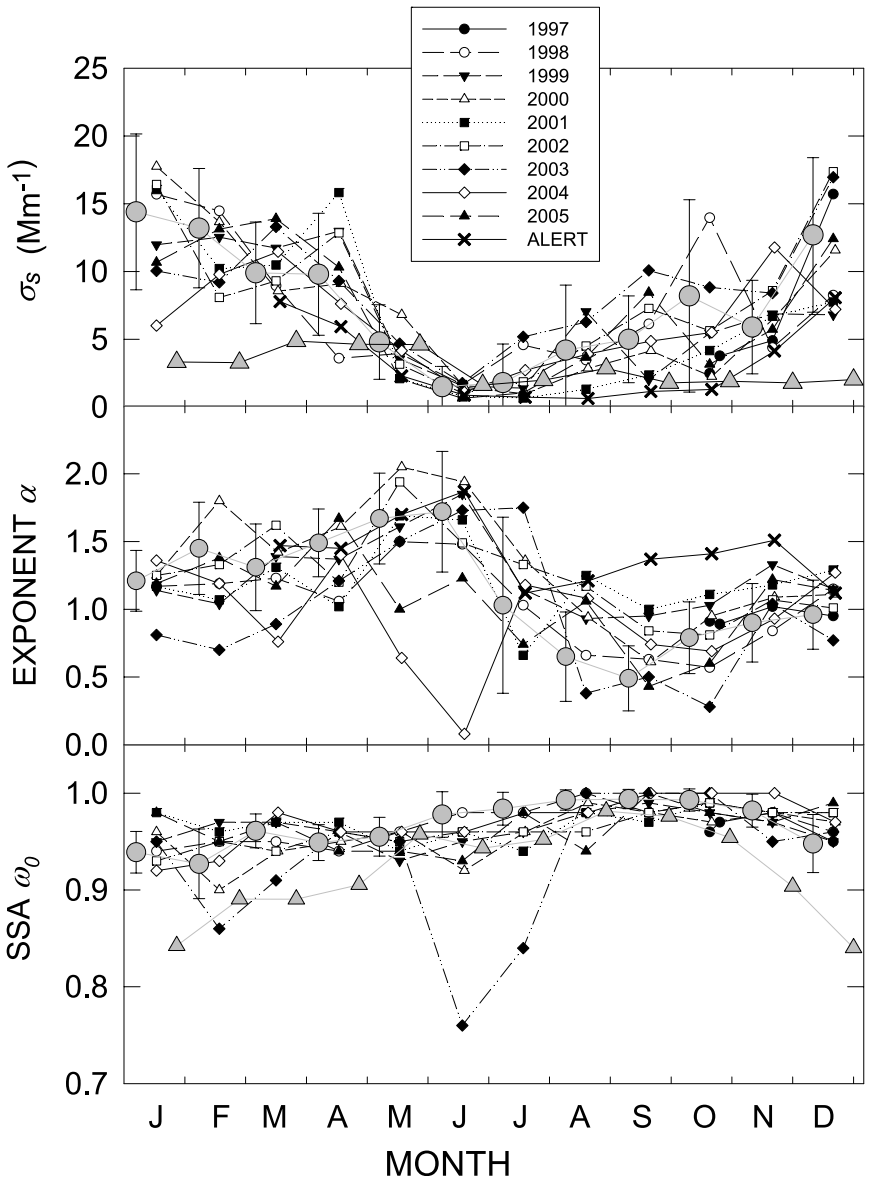

Figure 7. Annual cycles of the monthly mean values of aerosol volume scattering coefficient σ_s(550 nm), Ångström parameter α and single scattering albedo ω_o, measured at Barrow (open and solid symbols) in the years from 1997 to 2005 (from Barrow archive web page, ftp://ftp.cmdl.noaa.gov/aerosol/brw/archive/) and at Alert in 2006 (crosses). These data are compared with (1) the monthly median values of parameters σ_s(550 nm), α, and ω_o (shaded circles, with vertical bars defining the 1st and 3rd quartile values), as derived from the Barrow aerosol record over the period 1997–2000 [*Delene and Ogren*, 2002], and (2) the monthly mean values of parameters σ_s(550 nm) and ω_o measured at the Zeppelin (Ny Ålesund) station by the Stockholm University group throughout the period from late 1999 to July 2005 (shaded triangles).

spray. In the summer sulfate and sea salt both contribute to the submicron light scattering. Supermicron scattering tends to be dominated by sea salt particles and is most important in the summertime because of the break up of the sea ice. *Quinn et al.* [2007] show annual cycles in polar aerosol sulfate concentrations for Barrow, Alert and Arctic EMEP sites. A peak is observed during the springtime consistent with other indicators of Arctic haze. At most of the eight sites they studied there appears to have been a significant decrease in springtime non-sea-salt (nss) sulfate since 1980 and during the early 1990s. Over the more recent period from 1997 to the present, *Quinn et al.* [2007] found that the monthly average values of scattering coefficient σ_s(550 nm) for sub-10 μm aerosols measured at Barrow show an overall increase of about 50% in March and exhibit a more stable trend in April. Correspondingly, the monthly average values of aerosol nitrate concentration were found to increase at Alert (Canada) by about 50% between the early 1990s and 2003, presumably as a result of the expansion of the offshore oil and gas industry in the Arctic.

[22] Using aethalometer measurements made at Barrow and Alert, *Sharma et al.* [2006] showed that equivalent

black carbon (EBC) concentrations at the two sites show similar seasonal variation seen in AOD and σ_s at other Arctic sites. They reported values of about 100 ng m^{-3} at Alert and of 80–90 ng m^{-3} at Barrow, during the winter months, which then decreased at both sites from April to July, to assume values between 10 and 20 ng m^{-3} during the summer. *Sharma et al.* [2006] also present long-term trends in EBC over the 15 year period 1989–2003, suggesting a decrease of up to 50% in this period (2–3% per year), very similar to the decreasing trend observed in AOD. Correspondingly, the monthly median values of ω_o measured at Barrow were found to present the maximum in September ($\sim$0.98) and a wide minimum from February to May, with an average value of 0.94.

[23] From sampling measurements performed in 2000 and 2001 at the Zeppelin station using a Differential Mobility Particle Sizer (DMPS), the average particle number density size distribution curve was found to be substantially bimodal in March, when the occurrence of Arctic haze episodes is rather high, with mode diameters $D_p \approx 0.04$ μm and $D_p \approx 0.15$ μm, respectively, and monomodal in the other months, with $D_p \approx 0.04$ μm in June, $D_p \approx 0.08$ μm in September, and $D_p \approx 0.12$ μm in December [*Ström et al.*, 2003]. The corresponding monthly mean values of total number concentration of particles with diameters $D > 0.02$ μm were found to increase gradually from less than 100 cm^{-3} in January to more than 600 cm^{-3} in June, and then to decrease throughout the summer until assuming a minimum of about 80 cm^{-3} in October. Monthly median values of coefficients σ_s and σ_a for the visible light, measured at the Zeppelin station from the end of 1999 to July 2005, were also considered and are presented in Figure 7 for comparison with the Barrow data. The Zeppelin site tends to have much less aerosol, as indicated by the lower values of coefficient σ_s. Nonetheless, the seasonal pattern for Arctic haze can clearly be observed at this very clean site, where parameter ω_o was found to present monthly mean values comparable to those measured at Barrow during the late spring and summer period, as can be seen in Figure 7. In fact, it was observed to vary mainly between 0.94 and 0.98 in spring and summer, and to assume appreciably lower values in fall and winter, when it ranged between 0.84 and 0.91, presenting a marked minimum in December/January.

[24] Spectral measurements of σ_s were obtained at the Pallas GAW station, about 125 km northwest of Sodankylä, during the period from November 2001 to November 2004 [*Aaltonen et al.*, 2006b]. These in situ measurements showed considerably greater variation and the seasonal pattern was different from that typically observed at other Arctic sites. Parameter σ_s at the 550 nm wavelength was found to vary from 0.2 to 94.4 Mm^{-1}, with an yearly average value of 7.1 ± 8.6 Mm^{-1}, the scattering processes being dominated by submicron aerosols, especially during late summer and fall. Coefficient σ_s had a clear seasonal cycle, with a minimum in fall and 4–5 times higher maximum in summer. Parameter α also presented clear seasonal patterns, with maximum values in late summer and minimum values during wintertime, indicating that well aged accumulation particles produce predominant extinction effects on the solar radiation in winter and spring, while new and/or very small particles originating from coagulation processes are optically predominant in summer. The wide seasonal dispersion of data is presumably due to the long-range transport of particulate matter from the industrialized areas of the Kola Peninsula, Scandinavia and Russia as well as from the United Kingdom and Europe, with contributions from boreal forests [*Tunved et al.*, 2006].

[25] Comparisons of seasonal in situ measurements of aerosol properties at various Arctic sites show evidence of different impacts from anthropogenic source regions. The western Arctic shows a reduction in the anthropogenic component, while the eastern Arctic has retained relatively high concentrations of pollution aerosol at least during winter and spring.

2.4. Case Studies of Arctic Aerosol Events That Have Regional Climate Implications

[26] Relatively small increases in the particle concentration within the polar atmosphere can cause significant changes in the atmospheric transmissivity, which is usually very high for background conditions. The consequence of enhanced aerosol loading is a perturbation of the surface energy balance. Arctic haze is the best known example of this phenomenon, but other sources of aerosol are also of interest and have climate implications. One such perturbation results episodically when dust from distant deserts is transported into the Arctic. The predominant flow is from Asia and it is referred to as Asian dust [*Shaw*, 1983; *VanCuren and Cahill*, 2002; *Bory et al.*, 2003]. Another type of aerosol that impacts the Arctic radiation balance is the smoke generated by boreal forest fires in Siberia or North America [*Forster et al.*, 2001; *Damoah et al.*, 2004; *Stohl et al.*, 2006]. Biomass burning in the Eurasian region can also affect the Arctic radiation balance. Examples of these are discussed briefly in the following sections.

2.4.1. Asian Dust

[27] Incursions of Asian dust have occurred in the Arctic for many years, probably sometimes confused with Arctic haze and thus not extensively investigated. There is a growing interest in identifying such events and determining what direct and indirect effects they have on the Arctic climate through radiative forcing. There is a potential for an increased mobilization of dust in source regions as drying occurs because of warming over the Gobi Desert and adjacent regions, which is expected to enhance transport of this dust into the Arctic Basin associated with changing circulation patterns in the North Pacific. An intense episode of Asian dust transport (combined with haze) was observed at Barrow in spring 1976 by *Rahn et al.* [1977], who carefully analyzed the chemical composition of aerosol samples, finding that the background aerosol was pollution-derived, while the particles with diameters greater than roughly 0.4–0.8 μm were mainly crustal, the source area being identified as the Takla Makan and Gobi deserts in eastern Asia, where great dust storms frequently occur in spring.

[28] A recent study has documented one such event, quantifying the radiative effects produced by Asian dust over Barrow, Alaska [*Stone et al.*, 2005]. During spring 2002, dust storms occurred in the Gobi Desert region of Mongolia and lofted large amounts of dust into the atmosphere, which were subsequently transported eastward in a broad plume that reached the high-latitude regions of

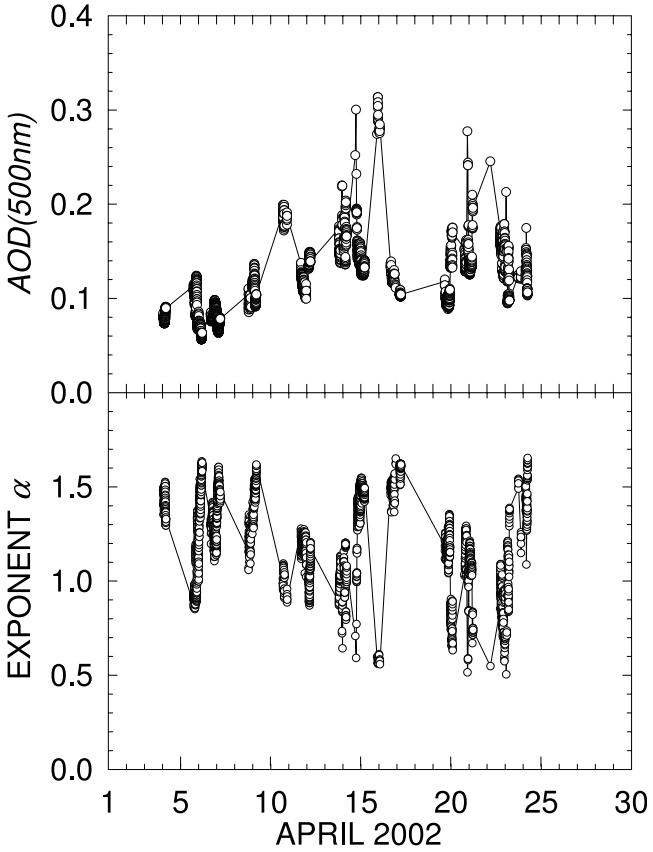

Figure 8. Time patterns of the 1-min values of AOD(500 nm) and Ångström exponent α, measured at Barrow by the NOAA/CMDL group in April 2002, during the sequence of Asian dust incursions over northern Alaska. They present a series of marked peaks of AOD(500 nm), clearly associated with evident minima of exponent α.

Northern America. Some of the dust was carried aloft by upper level winds following a trajectory passing over Barrow one week later, causing an increase in AOD at visible and near-IR wavelengths, which was measured by a NOAA/GMD Sun photometer. Figure 8 presents the time series of the 1-min values of AOD(500 nm) and corresponding Ångström exponent α measured at Barrow in April 2002. It shows that the arrival of Asian dust after 8 April caused a considerable increase in AOD(500 nm), from about 0.06 to 0.3 by mid-April. Simultaneously, a gradual lowering of α was observed from an average clean air value of about 1.4 to values close to 0.5.

[29] Because α is inversely related to the shape of the columnar aerosol size distribution (mean particle size), the low values of α shown in Figure 8 indicate the presence of larger particles, which in turn attenuate visible light very efficiently, causing the enhanced AOD(500 nm). The observations are consistent with a distribution of particles having (1) a broad accumulation mode of background particles, which alone might produce an α close to 1.4, and (2) a mode of larger (coarse) Asian dust particles. On the basis of lidar time series of backscattered light vertical profiles, the dust drifted overhead in layers having altitudes between 2 and 6 km. The size particle distribution was inferred from spectral AOD observations using an inversion algorithm [*King et al.*, 1978]. This analysis resolved the coarse mode with a mean diameter of about 2 μm.

[30] Assuming the above size distribution characteristics and a refractive index with real part equal to 1.51 and imaginary part equal to 0.009 at visible wavelengths [*Sokolik et al.*, 1993], instantaneous surface-level evaluations of direct aerosol radiative forcing (DARF) during the April 2002 event were obtained using the MODTRAN™ radiative transfer model. DARF, as defined in this study, is the change in net short-wave irradiance (down minus up) at the surface for a unit increase in AOD at 500 nm. Computations were made for a set of solar zenith angles for which empirical estimates of DARF were available by way of comparison. The range in angles was sufficient to capture and evaluate forcing over the diurnal cycle. Model values were found to range from -14 to -31 W m^{-2} per unit AOD(500 nm), for solar zenith angles from 81° to 62°, respectively, compared with values from -16 to -38 W m^{-2} for measured DARF. The rather consistent evaluations corroborate and quantify a strong cooling effect produced by Asian dust on the surface energy balance of the Arctic in spring. Should such episodes increase in frequency and/or intensity and be widely dispersed, the climate impacts of Asian dust may be underestimated when making climate assessments. This cooling effect is one example of a negative feedback, when viewed in the context of global warming in response to increasing concentrations of greenhouse gases.

2.4.2. Smoke From Boreal Forest Fires

[31] Other episodic occurrences at high northern latitudes are fires that burn vast areas of boreal forests across North America and Siberia each spring and summer. They have potentially far greater impact than dust storms because of the vast source regions and the expected increase in their frequency, duration and intensity as boreal zones continue to warm and dry. During the summer of 2004, for instance, over 5 million hectares of boreal forests burned in Alaska and Canada. *Stohl et al.* [2006] showed that the arrival of the smoke plumes above Barrow, Alert, Summit and Zeppelin stations produced rather marked peaks in the 3-hour mean light absorption coefficient, which coincided with the pronounced peaks of surface CO concentration simulated by the FLEXPART model, CO being a molecular species often used as a tracer of the smoke air masses. At Barrow, 3-hour mean values of σ_a were found to vary mostly between 0.5 and 1.5 Mm^{-1} during July, with a strong peak of about 32 Mm^{-1} on 3 July 2004, and typical background values close to 0.1 Mm^{-1}. As the smoke was transported across the Arctic, increases in absorption at both Alert (a few days later) and Ny Ålesund ($\sim$1 week later) were observed. The high values of the aerosol absorption coefficient will have had direct radiative effects, enhancing the atmospheric absorption of solar radiation.

[32] In order to obtain realistic evaluations of the DARF effects due to boreal smoke aerosols, it is necessary to know the spectral values of AOD associated with these highly absorbing aerosol particles, the size distribution, and the complex refractive index of particulate matter. Spectral measurements of AOD were carried out during July and August 2004 at Barrow, Summit and Ny Ålesund (AWI-

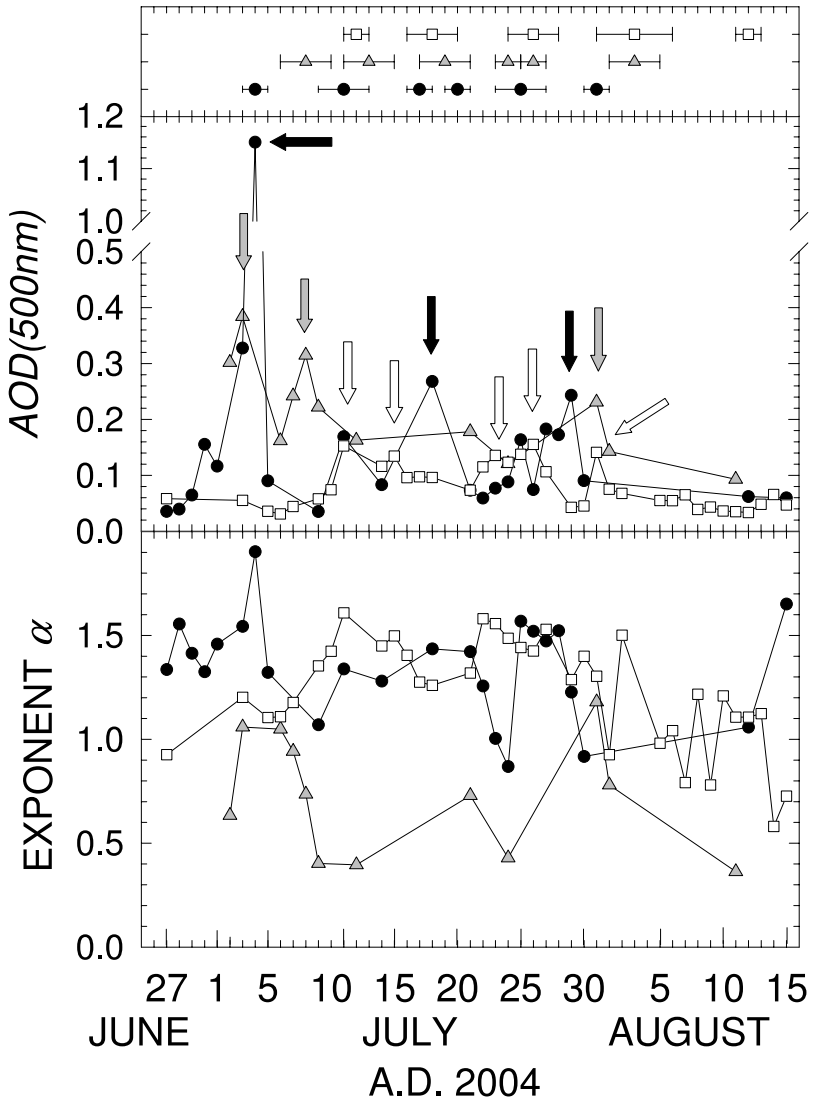

Figure 9. Time patterns of AOD(500 nm) and Ångström exponent α measured at Barrow (solid circles), Summit (shaded triangles) and Ny Ålesund AWIPEV (open squares) stations, during the period of boreal smoke transport over the Arctic region. Solid, shaded and open arrows indicate the AOD peaks due to the arrival of forest fire smoke above the three stations, respectively. The same symbols with bars shown in the top part of the graph indicate the periods during which peaks of CO concentration were measured at the three stations, this molecule being assumed to be a representative tracer of the forest fire smoke [*Stohl et al.*, 2006].

PEV). The time series of the daily mean values of AOD(500 nm) and derived Ångström exponent α measured at these three stations during that period are shown in Figure 9. They present a sequence of AOD(500 nm) peaks characterized by very high values at Barrow, as can be seen in Figure 3, which coincide closely with the peaks of surface CO concentrations modeled by *Stohl et al.* [2006] at the same sites, and marked in Figure 9 by means of symbols with horizontal bars. The different arrows indicate the simultaneous peaks of AOD(500 nm) measured at the three stations. Although in part limited by the presence of cloudy sky conditions on several measurement days, the three sequences clearly show that there is a delay of a few days between the Barrow and Summit peaks, while the Ny Ålesund peaks were measured about one week later. Correspondingly, the Barrow values of α were found to be mostly higher than unity throughout the whole summer period, suggesting that the fine particle fraction gave a considerable contribution to the columnar aerosol extinction of direct solar irradiance. The high concentration of fine particles was presumably due to the relative proximity of observation site and particle sources. Conversely, lower values of α were generally measured at both Summit and Ny Ålesund, possibly as a result of the particle growth occurring during the transport of the air masses over oceanic areas, from the emission regions to the observation sites, or of mixing with larger sea salt aerosols in transit. Preliminary evaluations of DARF for boreal smoke were made by *Key et al.* [2006] using the methods of *Stone et al.* [2005]. Like dust, boreal smoke was evaluated to cause a cooling effect

on the surface, which can be very significant, especially over the snow or ice-free surfaces prevailing over much of the Arctic by late summer. In fact, the evaluations of the surface DARF per unit AOD(500 nm) determined by *Key et al.* [2006] for an average case of boreal smoke, indicate that DARF can assume (1) values ranging between -45 and -18 W m^{-2} for solar zenith angle θ_s equal to 65° and surface albedo equal to 0.47 and 0.80, respectively, and (2) values ranging between -88 and -108 W m^{-2} for the same value of θ_s and surface albedo decreasing from 0.20 (tundra) to 0.02 (seawater). Thus boreal smoke is also a negative feedback that must be accounted for when making climate assessments.

2.4.3. Biomass Burning/Pollution Event

[33] One noteworthy pollutant transport event occurred in the Scandinavian Arctic on 2 and 3 May 2006, when daily mean values of AOD(500 nm) equal to 0.38 and 0.56 were measured, respectively. The very intense episode was caused by the massive transport of polluted air masses from Central Europe mixed with particle loads originating from agricultural fires in Eastern Europe (see Extreme transport episode web page, http://zardoz.nilu.no/~andreas/extreme_transport.gif), during which α assumed values close to 1.7, as shown in Figure 4, and β varied around 0.15. Simultaneously, relatively low visual range conditions of less than 20 km were observed. The volume particle extinction coefficient at the 532 nm wavelength was evaluated from lidar measurements to be close to 0.3 km^{-1} at the altitude of about 0.4 km, i.e., threefold higher than normally observed in other less intense Arctic haze episodes (with mean visual range of ~35 km), and around 6 times higher than that measured for clean air conditions (presenting mean visual range of more than 60 km), maintaining rather stable values up to an altitude over 2 km.

[34] During the period from late April to mid-May, particle samplings were collected at the Zeppelin station with the DMPS and the Optical Particle Counter (OPC) over the 0.02–0.84 μm and the 0.35–6.5 μm particle diameter range, respectively. A dry particulate mass concentration of around 10 μg m^{-3} was measured on 27 April 2006, assuming a mass density of 1.5 g cm^{-3}, while considerably higher values of around 30 μg m^{-3} were inferred on 2 May, and even higher values on 3 May, when peak hourly mean values of more than 50 μg m^{-3} were sometimes logged. The OPC data were in agreement, within 30%, with the DMPS measurements of particle number density. The chemical composition of the particulate matter was measured to vary appreciably from 23 April to 7 May 2006, with weekly mean mass percentages of sea salt of 38.7 and 9.0%, water soluble inorganic matter of 39.5 and 29.3%, water soluble organic matter of 16.5 and 50.6%, non-water-soluble organic matter of 2.9 and 8.9%, and elemental carbon of 2.4 and 2.1%, respectively. The relatively high values of the last composition parameter suggest that ω_o should have assumed considerably lower values than the monthly means determined in the period from 1999 to 2005 and shown in Figure 7. The DMPS measurements showed that a shift of the mode diameter from 0.16 to 0.20 μm occurred from 27 April to 2 May in the first accumulation mode, associated with a greater than two-fold increase in the number concentration. The AOD measurements performed on 4 May 2006 at the Rabben station for real humid atmosphere conditions at the coastal site of Ny Ålesund, yield a value of α close to 1.7, confirming that accumulation particles of relatively small sizes produced optically predominant effects along the vertical atmospheric path, during this unusual haze episode.

3. Aerosol Measurements in Antarctica

3.1. Antarctic AOD: Long-Term Trends Over the Last 30 Years

[35] The first AOD measurements in Antarctica were taken at the Norwegian station of Maudheim (71°03′S, 10°54′E, 38 m MSL) during the austral summer of 1950/1951, within a spectral channel centered at the 1 μm wavelength [*Lilijequist*, 1957]. In the 1960s–1980s, episodic measurements of the atmospheric turbidity parameters were performed using actinometers equipped with glass bandpass filters at Plateau in 1967/1968 [*Kuhn*, 1972], Mirny (Russia) in 1966–1969 and in 1979–1984, and Molodezhnaya (Russia) in 1977–1980 [*Radionov*, 1994; *Radionov et al.*, 2002]. More regular measurements of AOD have been inferred from global solar radiation data recorded at South Pole (USA) since 1976, employing pyrheliometers equipped with wideband interference filters (see Table 1), and from those measured episodically at McMurdo (USA, 77°51′S, 166°40′E, 10 m MSL) in 1977/1978. The first measurements of AOD performed in Antarctica using a Sun photometer model equipped with a set of narrow-band interference filters were taken at Mirny in 1968/1969 [*Sakunov and Rusin*, 1980].

[36] Over the last two decades, precise multiwavelength measurements of AOD have been performed at the coastal and low- and high-altitude Antarctic stations, using advanced Sun photometers. The coastal and inland stations where the measurements have been carried out are (1) Molodezhnaya in 1984 and 1986–1989, (2) Syowa (Japan) since 1985 [*Japan Meteorological Agency*, 2006], (3) Mirny since 1983, (4) "Mario Zucchelli" (Italy) at Terra Nova Bay in several austral summer periods from 1987/1988 to 2004/2005, (5) Georg-Forster (DDR/Germany) from 1988 to 1993, (6) Neumayer (Germany) since 1991, (7) Aboa (Finland) in January 2000, and (8) Marambio (Argentina) in the austral summer 2004/2005. The high-altitude sites are (1) Kohnen (Germany) in the austral summer periods of 2000/2001, 2001/2002 and 2005/2006; (2) South Pole since 2002; and (3) Dome C (France/Italy) in January of 2003 and 2006. The instruments used in the most recent years by the various groups are listed in Table 1.

[37] Figure 10 shows the historical series of the monthly mean values of AOD(500 nm) derived at (1) Mirny and Molodezhnaya stations, through actinometer and Sun photometer measurements performed from 1979/1980 to 2006 and from 1985 to 1989, respectively [*Radionov*, 1994; *Radionov et al.*, 2002], and (2) Neumayer AWI station from Sun photometer measurements carried out from 1991 to 2004. The time patterns of AOD(500 nm) are compared in Figure 10 with those of effective visible AOD$_{eff}$ derived from filtered pyrheliometer measurements performed at South Pole from 1977 to 2001 [*Dutton and Christy*, 1992; *Stone*, 2000]. The comparison offers evidence of the large variations caused by the formation of dense volcanic particle layers which were generated in the low stratosphere

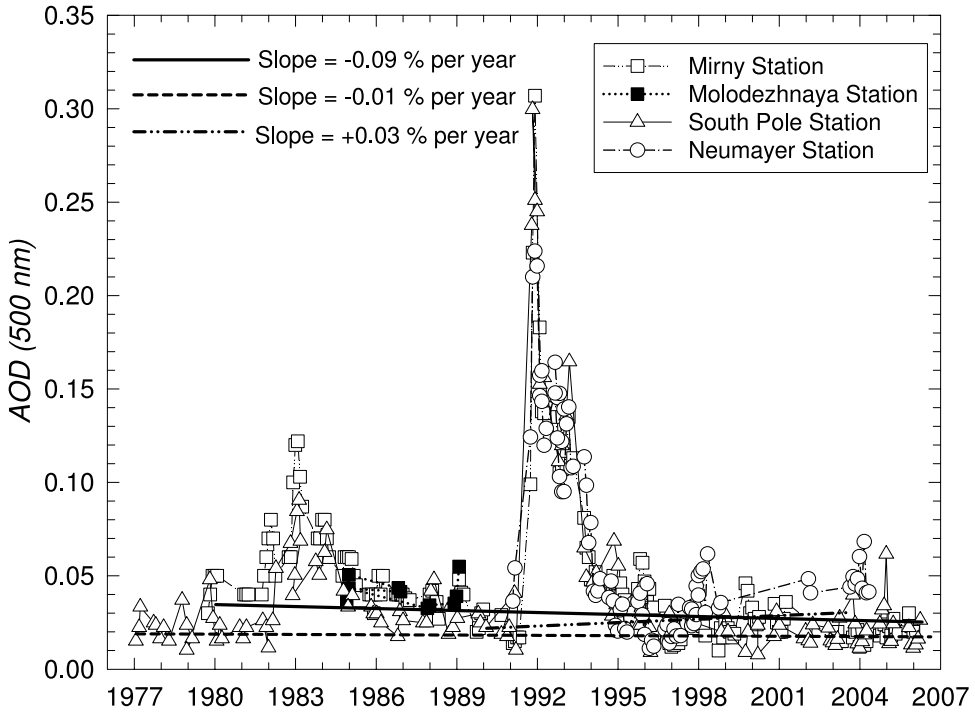

Figure 10. Time patterns of the monthly mean values of AOD(500 nm) derived from (1) filtered actinometer and Sun photometer measurements performed at Mirny (open squares), from austral summer 1979/1980 to that of 2005/2006, and at Molodezhnaya (solid squares) from 1985 to 1989; (2) filtered pyrheliometer and Sun photometer measurements taken at South Pole (open triangles), from 1977 to 2006; and (3) from Sun photometric measurements carried out at Neumayer (open circles), from 1991 to 2004. The regression lines, defined separately for the Mirny, South Pole and Neumayer data sets (without volcanic data), are drawn to show the long-term trend of background aerosol extinction in Antarctica.

by the El Chichon eruption in 1982, with monthly mean values of AOD(500 nm) higher than 0.10 in the austral summer 1982/1983 [*Shiobara et al.*, 1987; *Herber et al.*, 1993], and by the Pinatubo and Cerro Hudson eruptions in 1991, with values of AOD(500 nm) higher than 0.30 in the austral summer 1991/1992 [*Herber et al.*, 1996]. Considering the background values of AOD(500 nm) only, and omitting those measured during the field campaigns performed from 1982/1983 to 1984/1985 and from 1991/1992 to 1994/1995, which were all strongly affected by marked volcanic particle extinction effects, the regression lines were determined for the Mirny, South Pole and Neumayer data sets, in order to verify the existence of long-term trends in the Antarctic AOD records. The regression lines were determined for absolute regression coefficients ranging between 0.91 and 0.95, with slope coefficients equal to −0.09% per year at Mirny, −0.01% per year at South Pole, and +0.03% per year at Neumayer. Therefore the findings indicate that the extinction of solar radiation produced by the columnar Antarctic aerosols has been quite stable over the last 30 years, at both coastal and high-altitude sites, apart from the strong changes caused by the volcanic eruptions.

[38] The very weak trend for the South Pole AOD(500 nm) values agrees closely with the long-term trends of some surface radiative parameters determined at South Pole from the time series of surface-level nephelometer, performed routinely by the NOAA/GMD group (see South Pole archive web page, ftp://ftp.cmdl.noaa.gov/aerosol/spo/archive/).

3.2. Measurements of AOD and Ångström Exponent at the Antarctic Stations

[39] Regular measurements of the spectral values of AOD have been taken during several field campaigns performed at various Antarctic sites in the past two decades, using the advanced examples of multiwavelength Sun photometers listed in Table 1. The measurements were carried out at (1) five coastal sites (Terra Nova Bay, Mirny, Neumayer, Syowa, and Marambio), (2) a low-altitude inland site (Aboa), and (3) three high-altitude stations over the Antarctic Plateau (South Pole, Kohnen, and Dome C), during the periods defined in Table 3. Several spectral series of AOD were recorded on each measurement day at the various sites. For each spectral series of AOD, a pair of best fit values of α and β were determined following the *Ångström* [1964] best fit procedure or the two-wavelength method described in subsection 2.2. Some examples of the Ångström procedure are shown in Figure 11, applied to spectral series of AOD measured at the Neumayer, Kohnen and Terra Nova Bay sites, providing best fit values of α varying from 0.61 to 1.85, obtained for regression coefficients better than −0.96. Figure 11 also presents some examples of the good accuracy reached by the ISAC-CNR and AWI Sun photometers (Table 1) in measuring the spectral values of AOD, estimated to be of around 0.01

Table 3. Evaluations of the Overall Ranges and Median Values of Parameters AOD(500 nm), α and β Obtained From the Data Sets Measured at Nine Antarctic Stations and presented in Figures 12–14

		AOD(500 nm)		Exponent α		Parameter β	
Station	Measurement Period	Range	Median	Range	Median	Range	Median
Terra Nova Bay	1987/1988 to 2004/2005	0.010–0.084	0.039	0.02–2.10	0.94	0.002–0.054	0.023
Marambio	February 2005 to May 2005	0.018–0.097	0.029	0.17–1.35	0.73	0.007–0.084	0.013
Aboa	January 2000	0.035–0.063	0.051	1.66–1.87	1.75	0.011–0.019	0.014
Neumayer	1993/1994 to 2003/2004	0.008–0.220	0.060	−0.62–2.54	0.64	0.006–0.105	0.024
Mirny	1993/1994 to 2005	0.015–0.105	0.042	0.30–2.48	0.77	0.003–0.079	0.023
Syowa	1993/1994 to 2001	0.006–0.085	0.022	−0.40–2.45	1.10	0.002–0.059	0.010
Kohnen	2001/2002 to 2005/2006	0.007–0.028	0.015	0.45–3.02	1.66	0.002–0.015	0.005
Dome C	January 2003 and 2006	0.015–0.027	0.019	1.13–1.98	1.61	0.004–0.012	0.006
South Pole	2001/2002 to 2005/2006	0.009–0.034	0.015	0.87–2.28	1.70	0.002–0.017	0.005

within all the visible and near-infrared channels, for both sea level and high-altitude atmospheric transparency conditions.

[40] From the daily sets of AOD(500 nm), α and β obtained during each campaign and at each site, the daily mean values of the three parameters were then calculated, over the period from the austral summer of 1993/1994 to that of 2005/2006. The results are presented in Figures 12 and 13 for the coastal and low-altitude stations and in Figure 14 for the high plateau stations. The time patterns of daily mean values of AOD(500 nm) defined during the various campaigns are shown in Figures 12–14, giving an overall picture of the seasonal variations of this columnar quantity usually occurring in Antarctica for austral summer clear-sky conditions [*Tomasi et al.*, 1989, 1991; *Vitale and Tomasi*, 1990; *Herber et al.*, 1993, 1996; *Radionov et al.*, 1994, 2002; *Cacciari et al.*, 2000; *Virkkula et al.*, 2000; *Di Carmine et al.*, 2005; *Japan Meteorological Agency*, 2006]. These values of AOD(500 nm) were found to range mainly between 0.02 and 0.06 at the coastal and low-altitude sites, presenting considerably higher values during the austral summer of 1993/1994, when appreciable columnar loadings of volcanic particles were still suspended in the Antarctic atmosphere. The corresponding values of α were widely scattered throughout the range from 0.2 to more than 2, the values lower than 0.5 being often due to the significant extinction effects produced by aged volcanic aerosol layers and associated with appreciably higher values of β than

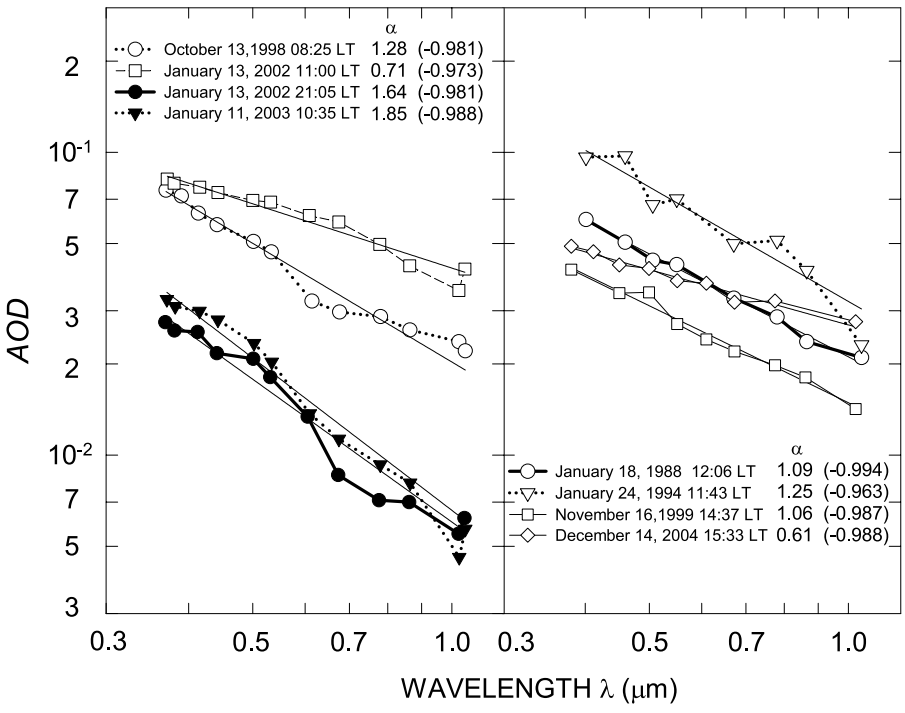

Figure 11. (left) Examples of the *Ångström* [1964] best fit procedure applied to two pairs of AOD spectral series measured at the AWI Neumayer (open symbols) and AWI Kohnen (solid symbols) stations in Antarctica, using the SP1A and SP2H Sun photometers [*Herber et al.*, 2002]. (right) As in Figure 11 (left), for four AOD spectral series measured at the "Mario Zucchelli" Terra Nova Bay station (Italy), using the UVISIR-2 (open circles and triangles), and ASP-15WL Sun photometers (open squares and diamonds) [*Tomasi et al.*, 1989; *Cacciari et al.*, 2000]. The best fit values of exponent α are also given for all the eight examples, together with the corresponding regression coefficients (in brackets).

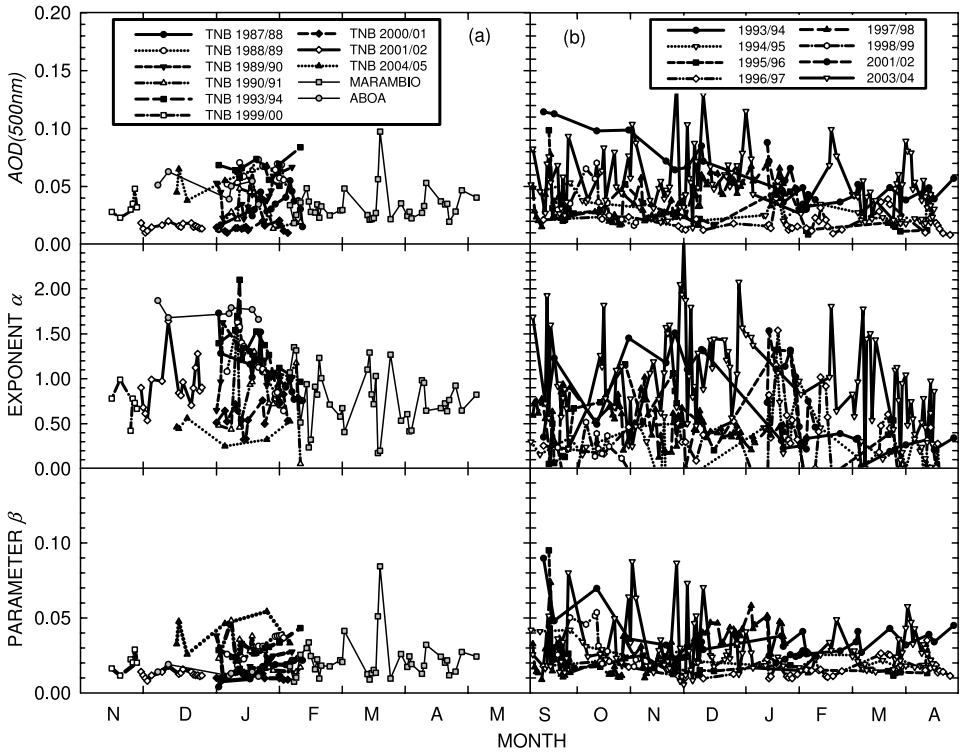

Figure 12. (left) Seasonal time patterns of the daily mean values of AOD(500 nm), exponent α and parameter β, obtained from the Sun photometer measurements taken at Terra Nova Bay (TNB) during nine austral summer campaigns from 1987/1988 to 2004/2005 (open and solid symbols), Marambio (Finland) in austral summer 2004/2005 (shaded squares), and Aboa (Finland) in January 2000 (shaded circles). (right) As in Figure 12 (left) for the Sun photometer measurements performed at Neumayer during nine field campaigns from 1993/1994 to 2003/2004 (open and solid symbols).

those measured for background conditions of atmospheric turbidity. In fact, β assumed values ranging mainly between 0.005 and 0.04 in the absence of the Pinatubo and Cerro Hudson particle extinction, and greatly exceeded 0.04 during the austral summer of 1993/1994 at the various sites.

[41] The daily mean values of AOD(500 nm), α and β measured at the high-altitude stations of South Pole, Kohnen and Dome C are presented in Figure 14, showing values of AOD(500 nm) ranging mainly between 0.005 and 0.03, with α varying mostly between 1.0 and 2.2, and β between 0.002 and 0.01, for cloudless sky conditions. The values of AOD(500 nm) > 0.05, which turn out to be associated with $\alpha < 0.5$ and $\beta > 0.02$, are presumably given by the sum of two terms, the first due to a background aerosol loading and the latter to the presence of thin cirrus clouds not easily visible to the naked eye, or ice crystal layers often present in the Antarctic atmosphere.

[42] The sets of daily mean values of AOD(500 nm), α and β, shown in Figures 12–14 were then examined to define their overall range and evaluate their median values, separately for the nine Antarctic stations. The resulting data are given in Table 3, and are suitable for defining average extinction models of Antarctic aerosols. The comparison between the daily mean values of AOD(500 nm), α and β measured at the three high-altitude stations and those determined at the coastal and low-altitude stations clearly shows that the values of AOD(500 nm) measured on the Antarctic Plateau are in general lower by at least 50% than those measured at the sea level sites [*Vitale and Radionov*, 2005]. In fact, AOD(500 nm) exhibits median values varying between 0.02 and 0.06 at the coastal sites and lower than 0.02 at the high plateau stations, while α assumed median values ranging between 0.4 and 1.1 at the coastal sites and between 1.6 and 1.7 at the Antarctic Plateau sites. Values of $\alpha > 1.5$ can be assumed to indicate the optical predominance of fine particles on large and coarse particles, while values of $\alpha < 1.1$ could indicate the optical predominance of the large accumulation and coarse particles. These concepts were mentioned in the previous section when discussing the spectral dependence of Arctic haze and Asian dust extinction effects on the shape parameters of the multimodal particle size distribution. Thus the evaluations of the median values of α given in Table 3 indicate that accumulation particles are in general optically predominant at the coastal sites, while fine particles produce prevailing extinction effects at the high plateau sites.

3.3. In Situ Measurements of Chemical Composition and Radiative Properties of Aerosol at the Coastal and Low-Altitude Sites

[43] The aerosol radiative properties are closely related to the origins and chemical composition of particulate matter [*Hänel and Bullrich*, 1978]. In Antarctica, where the relative humidity conditions of air are usually low on the austral summer clear-sky days, the water uptake of aerosol particles by condensation is generally very poor. Therefore the

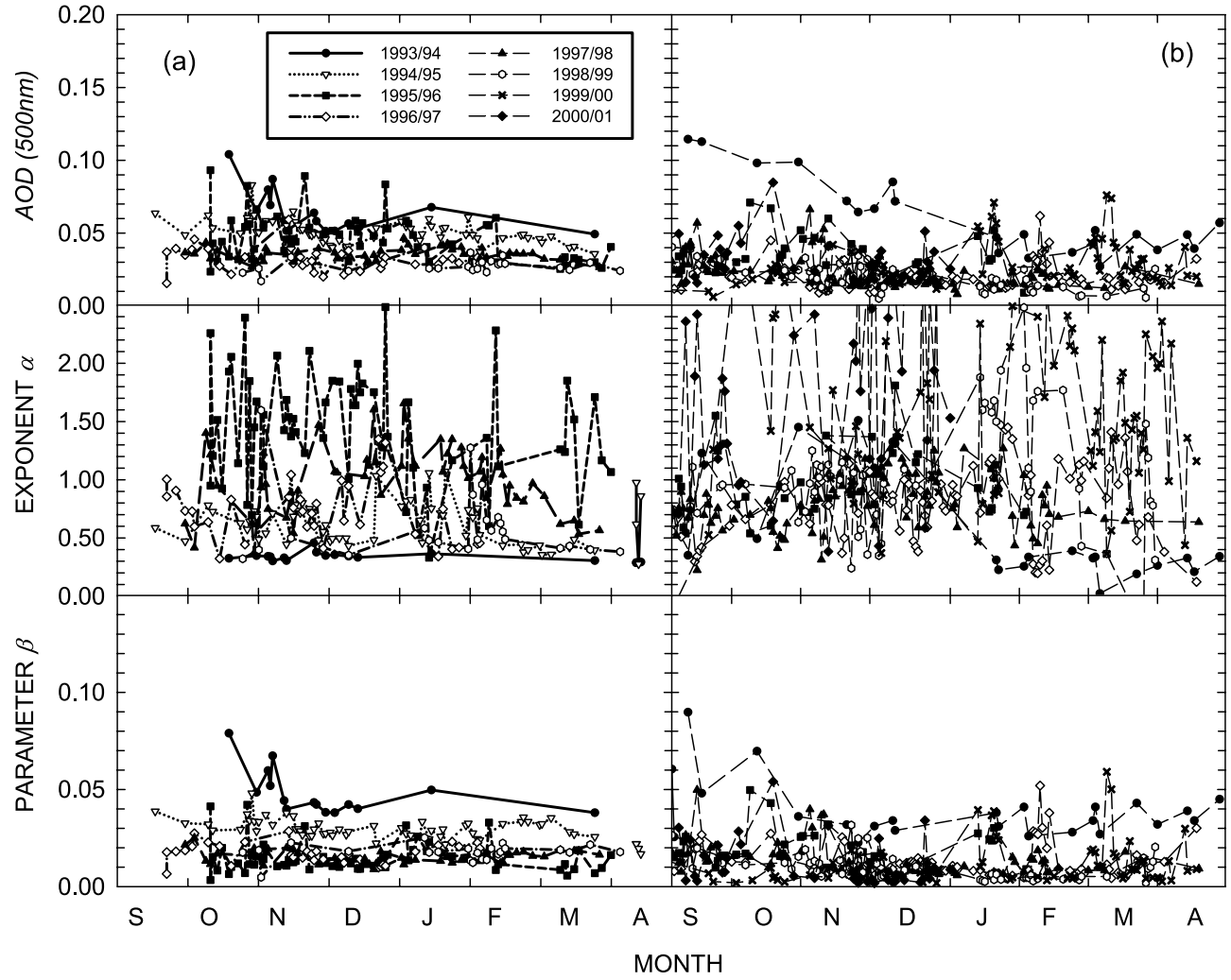

Figure 13. (a) Seasonal time patterns of the daily mean values of AOD(500 nm), exponent α and parameter β, measured at Mirny (Russia) during six field campaigns from 1993/1994 to 1998/1999 [*Radionov et al.*, 2002]. (b) As in Figure 13a for the Sun photometer measurements taken at Syowa (Japan) during seven campaigns from 1993/1994 to 2000/2001 [*Gernandt et al.*, 1996; *Japan Meteorological Agency*, 2006].

refractive index of particulate matter strongly depends on the dry-air mass fractions of its constituents. Considering the optical predominance of large and coarse particles at coastal sites, and of fine particles at continental sites, the chemical composition of Antarctic aerosols has been closely investigated by several groups in the recent years, to define the mass fractions of the substances forming the aerosol particles within the various size classes, at both coastal sites (Terra Nova Bay, Syowa, Neumayer, Halley) and low- and high-altitude stations (Aboa, Kohnen, Dome Fuji, South Pole).

[44] At Terra Nova Bay, *Hillamo et al.* [1998] carried out measurements of the mass concentrations of major inorganic ions in aerosol particles and their atmospheric precursor gases, from late January to mid-February 1995, using the instruments in Table 2, to collect size-segregated particle samples over the 0.035–16 μm aerodynamic diameter range. The total mass concentration of inorganic ions in aerosols was estimated to vary most frequently between 2 and 2.5 μg m^{-3}, with particle size distributions usually presenting four modes: (1) a mode of Aitken nuclei and fine particles, with mode diameter D_p = 0.07 μm, giving a relative mass contribution of ~1% to the total mass content, in which ~35% is given by non-sea-salt (nss) sulfate, ~35% by chloride Cl^-, ~19% by ammonium (NH_4^+) and ~11% by nitrate (NO_3^-), these particles originating mainly from biogenic sulfur; (2) an accumulation particle mode ($D_p \approx 0.30$ μm) with a relative mass contribution of 14%, in which the predominant content is provided by nss $SO_4^=$ (~72%) and lower percentages by sea salt ions (10% Cl^- and 9% Na^+), NH_4^+ (5%) and NO_3^- (2%); (3) a large particle mode, with $D_p \approx 2$ μm and a relative mass content of 22%, in which the predominant contribution is given by sea salt ions (46% Cl^- and 30% Na^+) and by $SO_4^=$ (15%), with lower percentages by NO_3^-, Mg^{++} and NH_4^+; and (4) a coarse particle mode, with $D_p \approx 6.5$ μm, yielding 63% of the total mass, which consists mainly of sea salt (53% Cl^- and 33% Na^+), with ~10% by $SO_4^=$ and lower percentages of Mg^{++},

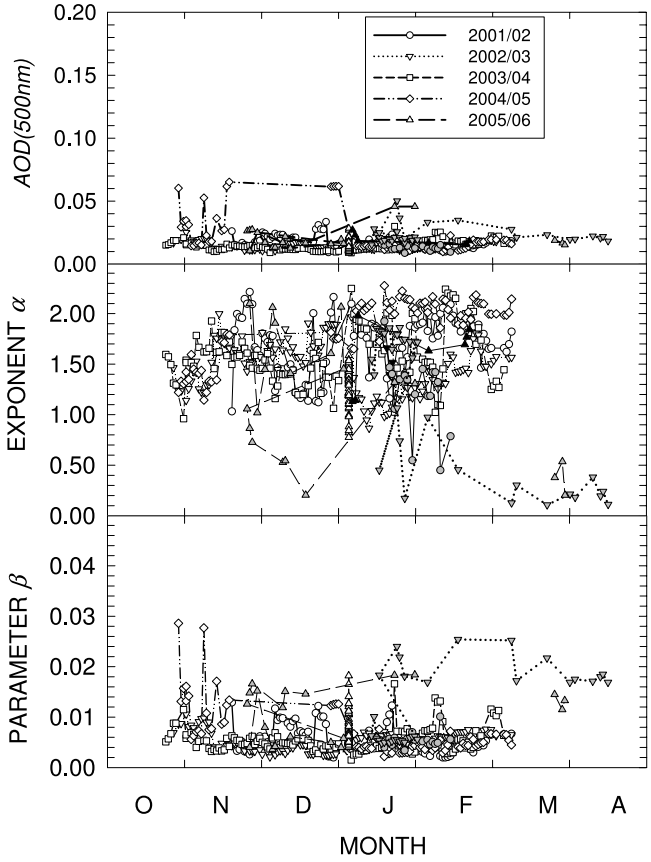

Figure 14. Seasonal time patterns of the daily mean values of AOD(500 nm), exponent α and parameter β, obtained from the Sun photometer measurements performed at the high-altitude stations of Dome C (France/Italy) in January 2003 and January 2006 (solid symbols), South Pole (USA) from 2001/2002 to 2005/2006 (open symbols), and Kohnen (Germany) in three field campaigns from 2001/2002 to 2005/2006 (shaded symbols).

NO_3^- and NH_4^+. The results indicate that the sulfates present in the two modes of larger particles are mainly formed through reactions between sea salt and atmospheric SO_2, the abundance of Cl^-, Na^+, Mg^{++} and NO_3^- ions being due to heterogeneous reactions of sea-salt particles with several gaseous compounds. For the above mass composition percentages, *Cacciari et al.* [2000] calculated the spectral values of the real part n and imaginary part k of the columnar particulate refractive index, separately for the various modes, finding values of n ranging mainly between 1.4 (4th mode) and 1.5 (2nd mode) and values of k varying between 1.4×10^{-3} (4th mode) and 5.4×10^{-3} (3rd mode), for which ω_o was estimated to vary on average between 0.97 and 0.99.

[45] Observations of aerosol constituents and acidic gases at Syowa showed that sea-salt concentration decreased to background levels in summer, presenting rather high values in winter due to blizzard and strong wind effects. Particulate Cl^- and Br^- are liberated preferentially from sea-salt particles in summer, the molar ratio Cl^-/Na^+ and Br^-/Na^+ usually decreasing to less than 0.5 [*Hara et al.*, 2004, 2005].

[46] At the coastal site of Neumayer, the average aerosol mass concentration at the surface was estimated to be equal to 1.3 μg m^{-3} in the austral summer, and 1.1 μg m^{-3} in the austral winter. The average chemical composition of particulate mass during the austral summer was found to consist of mass percentages equal to 48% sea salt, 33% nss sulfate, 12% methane sulfonic acid (MSA), and minor fractions of nitrates, mineral dust and ammonium. Conversely, a very high average percentage of 93% sea salt was measured in the austral winter, together with low percentages of a few percents due to nss sulfate, nitrate, MSA, ammonium and mineral dust [*Minikin et al.*, 1998]. A high correlation between nss sulfate and MSA concentrations was found on examining the time series of surface concentrations of the two substances, as recorded from 1983 to 1996, which are characterized by regular sequences of pronounced peaks in the austral summer months, both these biogenic sulfur aerosol components being atmospheric products of the dimethyl sulfide (DMS).

[47] Aerosol black carbon (BC) concentration was regularly measured by *Wolff and Cachier* [1998] with aethalometers, routinely operated at the British Antarctic Survey station of Halley (75°35′S, 26°32′W, 37 m MSL) on the Weddell Sea coast from 1992 to 1995. The measurements showed that BC concentration assumed daily mean values varying mainly between 0.3 and 2.0 ng m^{-3} throughout the year, with an yearly mean value close to 1 ng m^{-3}. This parameter followed a clear seasonal cycle, with a wide minimum from March to August ($\sim$0.6 ng m^{-3}), and an overall maximum of $\sim$1.5 ng m^{-3} in the period from October to February. The values were slightly higher than those recorded at South Pole. It is important to notice that they follow a pattern similar to that observed at South Pole as well as to that of mineral dust at Neumayer, suggesting that the BC concentration measured at Halley is actually controlled by the timing of biomass burning in the tropics, strongly modulated by the efficiency of transport to Antarctica.

[48] The chemistry of sea salt was also studied in depth at the low-altitude station of Aboa, about 150 km from the Atlantic coast in Queen Maud Land, through aerosol sampling measurements performed routinely from December 1997 to February 1998, using the instruments listed in Table 2 [*Kerminen et al.*, 2000; *Teinilä et al.*, 2000; *Koponen et al.*, 2003]. Sea salt particle concentration presented considerably lower values than those commonly measured at Terra Nova Bay and Neumayer. The average particle size distribution curve had multimodal features in most cases, throughout the particle diameter range from 0.045 to 15 μm, consisting in general of five principal modes: (1) a first mode of fine particles, with D_p varying between 0.03 and 0.10 μm, and mass percentages of 63% nss sulfate, 29% NH_4^+, and 8% MSA; (2) two accumulation particle modes, with average values of D_p close to 0.30 μm and 0.65 μm, consisting of 57–66% nss $SO_4^=$, 21–23% MSA, and 11–16% NH_4^+, with relatively low percentages of sea salt ions Cl^- and Na^+; (3) a large particle mode, with D_p varying between 1.4 and 1.9 μm, with predominant contents of sea salt (40% Na^+ and 12% Cl^-), nss sulfate (27%), MSA (12%) and lower percentages of NO_3^- and NH_4^+; and (4) a coarse particle mode, with D_p varying between 2 and 5 μm, which consists of sea salt (37% Cl^- and 26% Na^+), NO_3^-

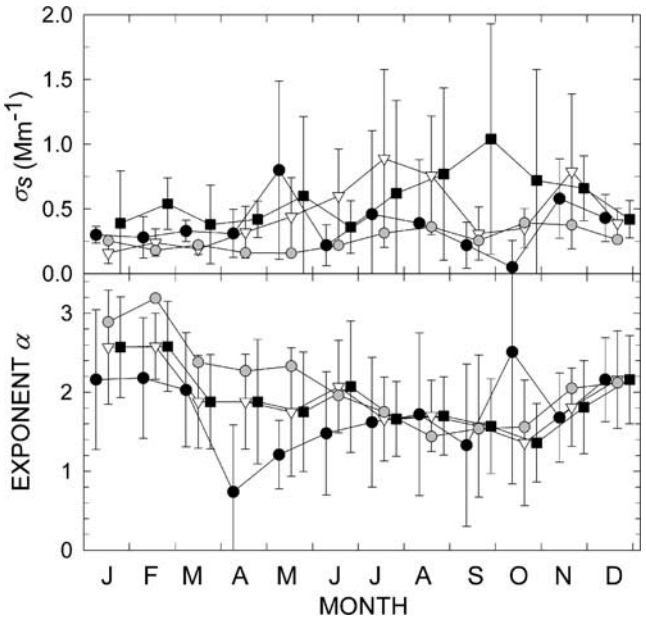

Figure 15. Annual cycles of the monthly mean values of the aerosol volume scattering coefficient σ_s(550 nm) and Ångström parameter α, with their standard deviations (vertical bars), measured at South Pole (South Pole archive web page, ftp://ftp.cmdl.noaa.gov/aerosol/spo/archive/) in 2003 (solid circles), 2004 (open triangles) and 2005 (solid squares). These time patterns are compared with the monthly medians of the same parameters determined by *Bodhaine* [1995] in 1987 (shaded circles).

(16%), nss sulfate (14%), MSA (5%) and NH_4^+ (2%). Thus more than 60% of the overall content of sea salt ions was detected in the supermicron size range, with higher percentages in the large particle mode. By contrast, the sea-salt particles displayed a large chloride loss with respect to the bulk seawater in the submicron range, mainly caused by primary ions like sulfate, nitrate, and MSA. Here, within the range of the submicron particles, the biogenic sulfur compounds were estimated to contribute by more than 90% to the aerosol mass concentration, while they compose on average only 30% and 50% of the coarse and large accumulation particle mass, respectively. These results were substantially confirmed by the Aboa measurements performed by *Virkkula et al.* [2006a] in January 2000, using a 12-stage low-pressure impactor, which defined the presence of both sea salt and nitrate modes centered at diameters D_p equal to 0.8 μm and $\sim$3 μm for sea salt, and D_p equal to 1.2 μm and $\sim$3 μm for nitrates, respectively.

[49] Applying both optical and chemical methods to these field measurements of the particulate composition, *Virkkula et al.* [2006b] found that the size-fractionated real part n of refractive index assumed an average value of 1.557 in the size range $8.5 \leq D \leq 15.0$ μm, and decreased gradually with D to reach average values of 1.511 for $1.06 \leq D \leq 1.66$ μm, 1.458 for $0.23 \leq D \leq 0.34$ μm, and 1.505 for $0.045 \leq D \leq 0.086$ μm. Parameter n of submicron aerosols was estimated to vary as a function of wavelength, being equal to 1.467 ± 0.039 at 450 nm, 1.454 ± 0.040 at 550 nm, and 1.460 ± 0.063 at 700 nm, for $k = 0$, excluding two nucleation episodes presenting anomalously low values of n, which lowered the above average values by about 0.02. However, a value of k no higher than 10^{-2} would have been more realistic, considering that (1) the Aboa aethalometer measurements of the submicron BC concentration were calculated assuming the mass absorption efficiency of 14 m^2 g^{-1}, and (2) about 93% of the observed values of ω_o were evaluated to be higher than 0.95, with only 3.5% of values lower than 0.90. Thus the above evaluations of the real part n should be only slightly underestimated, by no more than 1%.

[50] On the basis of the above results, it appears credible that the fine and accumulation particle modes are characterized by prevailing radiative properties due to sulfates and MSA, while the large accumulation and coarse particle modes should be characterized by the predominance of the sea salt and nitrate radiative properties.

3.4. In Situ Measurements of Chemical Composition and Radiative Properties of Aerosols at the High Plateau Sites

[51] The mean ionic composition of aerosol at Kohnen was measured by *Piel* [2004], finding average values of the relative mass percentages equal to $\sim$70% nss sulfate, 10% MSA, 8% NO_3^-, 3% Cl^- and 7% cations, during the austral summer. The sea salt aerosol concentration was lower by an order of magnitude than that measured at the coastal sites. These results were confirmed by *Hara et al.* [2004], who found that the background summer concentration of Na^+ at Dome Fuji was on average equal to $\sim$0.4 nmol m^{-3}, against a mean value of around 4 nmol m^{-3} measured at Syowa. In fact, the prominent role in aerosol formation is played at the high-altitude sites by the biogenic sulfur compounds and not by sea salt, a high correlation existing between nss sulfate and MSA concentrations [*de Mora et al.*, 1997]. The two biogenic sulphur products account for about 80% of the total aerosol mass, indicating that the Antarctic Plateau atmosphere is strongly influenced by the subsidence of aerosols from the free troposphere, during long-range transport [*Bigg*, 1980]. As a consequence of the prevailing amount of the two biogenic sulfur products, the high plateau aerosols show a high acidity, leading to large fractions of gas phase chloride (with 70–88% of HCl) and nitrate (with 53–67% of HNO_3).

[52] The monthly mean values of parameters σ_s for the visible light and exponent α were evaluated from the series of daily measurements performed by NOAA/CMDL at South Pole, from 2003 to 2005, using the instruments listed in Table 2. They are presented in Figure 15 (South Pole archive web page, ftp://ftp.cmdl.noaa.gov/aerosol/spo/archive/), indicating that coefficient σ_s varied between 0.2 and 0.6 Mm^{-1} during the austral summer, and between less than 0.1 and more than 0.8 Mm^{-1} in the austral winter, describing a seasonal cycle with a marked maximum from July to September. The present results turn out to be appreciably higher than the monthly medians measured by *Bodhaine* [1995] in 1987. At the same time, exponent α was found to assume values higher than 2 in the austral summer and mainly ranging between 1.5 and 2 in the austral winter, in accordance with the *Bodhaine* [1995] results. Both parameters exhibit a marked year-to-year variability, presumably related to the frequency of the sea salt aerosol

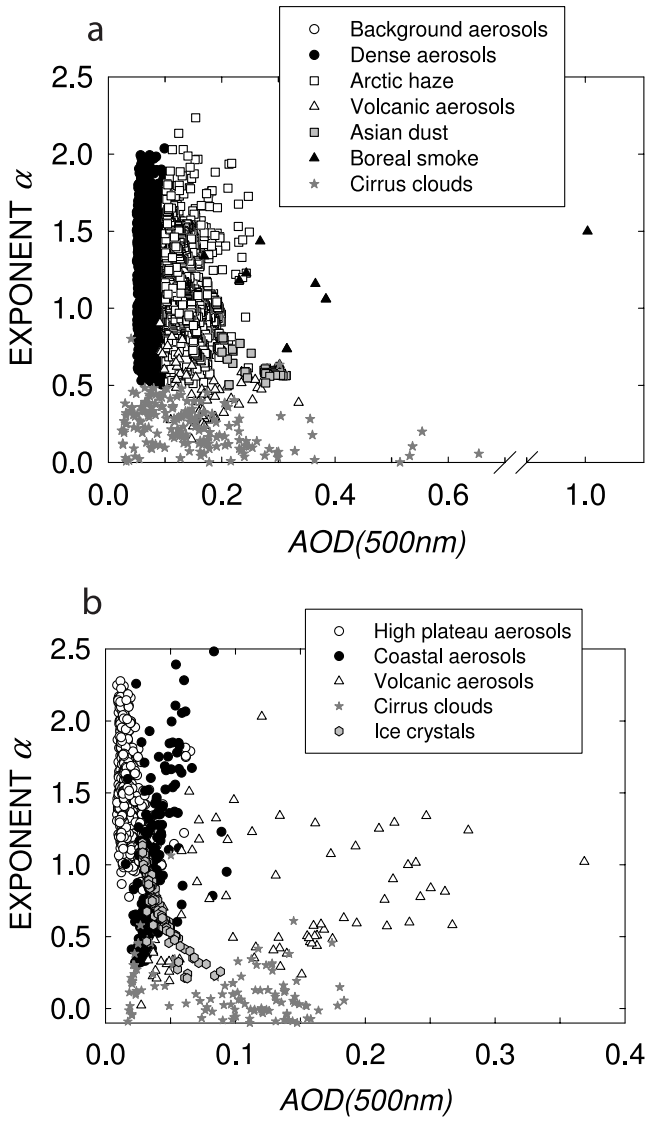

Figure 16. (a) Plot of the daily mean values of the Ångström exponent α as a function of the corresponding daily mean values of aerosol optical depth AOD(500 nm), for different classes of columnar Arctic aerosols and cirrus clouds of various optical depth. (b) As in Figure 16a, for different classes of columnar Antarctic aerosols, cirrus clouds and ice crystal layers of various optical depth. The ice crystal class also includes cases of "diamond dust" present near the surface, often observed at the South Pole under clear skies [*Town et al.*, 2005].

transport episodes from the coastal regions to continental Antarctica.

[53] In examining these results, it is important to bear in mind that the transport processes from the coastal regions of Antarctica can also involve air masses from midlatitude regions, generally containing significant loads of particulate matter generated by biomass burning and tropical forest fires. *Wolff and Cachier* [1998] evaluated that the yearly mean value of BC concentration at South Pole is equal to 0.6 ng m^{-3}, presenting a maximum of about 1.5 ng m^{-3} in January and a wide minimum of 0.2–0.3 ng m^{-3} from March to July. Thus the columnar aerosol loading observed at South Pole during the austral summer is estimated to consist mainly of fine sulfate aerosols, giving values of the real part n of refractive index ranging mainly between 1.50 and 1.58, with a mean value of 1.54 [*Hogan et al.*, 1979], together with values of $k < 10^{-2}$ at the visible wavelengths. Correspondingly, the austral summer values of ω_o were found to range mainly between 0.94 and 0.99, with an annual mean value of 0.97 [*Bodhaine*, 1995]. In fact, the intrusions of sea salt aerosols are observed only occasionally at South Pole, when particularly intense storms reach the interior from the surrounding ocean regions [*Bodhaine*, 1992, 1996]. In such cases, clear signatures distinguish the air masses carrying coarse (sodium) and small (sulfate) particles, with sodium concentration peaks associated with flow from the Weddell and Ross sea regions [*Shaw*, 1988]. By contrast, rather high summertime values of α are usually found, which can be explained in terms of the optical predominance of the fine sulfate particle mode [*Bergin et al.*, 1998].

[54] The present analysis of the chemical composition characteristics and radiative properties of Antarctic aerosols measured at coastal and continental sites leads to the conclusion that large differences exist between the columnar aerosol contents of the coastal and high-altitude stations. In particular, the coastal sites turn out to be strongly influenced by the surrounding ocean and, hence, the aerosol size distributions exhibit usually a strong component of large sea-salt particles during the austral summer. Conversely, the Antarctic Plateau stations are most frequently influenced by the subsidence of aerosols from the free troposphere, associated with long-range transport processes [*Bigg*, 1980] and are, consequently, characterized by prevailing contents of fine nss sulfate and MSA particles [*Hara et al.*, 2004]. Here, sea-salt aerosols are expected to present relevant concentrations at South Pole only when marine air is transported above the station by large storm systems [*Shaw*, 1988; *Bodhaine*, 1992].

4. Characterization of the Polar Aerosols

[55] The above results clearly suggest that polar aerosol can be characterized by large variations in their optical, physical and chemical composition parameters, causing a wide variety of particulate radiative properties throughout the year. Because the variable radiative effects caused by aerosols can influence the energy balance of the surface-atmosphere system quite significantly, there is a need to improve the optical parameterizations of the diverse aerosol species present in polar regions in order to quantify their radiative effects with greater accuracy.

[56] To provide evidence of the relationships between the size distribution features and the spectral characteristics of aerosol extinction, the daily mean values of Ångström's exponent α are plotted as a function of the corresponding values of AOD(500 nm) in Figures 16a and 16b, for the various polar aerosol classes found here to be present in the Arctic and Antarctic atmosphere. Although characterized by a large scatter of data, the plot of the Arctic data in Figure 16a shows that there is a general tendency for exponent α to decrease as parameter AOD increases, presenting (1) a large variability in the background aerosol,

dense aerosol and Arctic haze data, measured at eight stations; (2) values closer to unity in the Asian dust cases observed at Barrow, and in the boreal smoke cases, measured at Barrow, Summit and Ny Ålesund; and (3) values appreciably lower than unity in the aged volcanic aerosol data measured from 1991 to 1994. In particular, the data pertaining to the background aerosol, dense aerosol and Arctic haze classes were found to differ considerably, since they were grouped within different intervals of AOD but cover the same range of α, extended from 0.5 to more than 2. Cirrus clouds were found to constitute a well defined cluster, in which the values of α are in general low and mainly close to zero, corresponding to values of AOD(500 nm) falling in the majority of cases within the 0.0–0.2 range. To illustrate the variable dependence features, *Delene and Ogren* [2002] showed that a similar relationship also exists between the aerosol radiative parameters measured at the surface level, i.e., parameter α measured on the basis of nephelometer measurements of the volume scattering coefficient σ_s at the 550 and 700 nm wavelengths, and volume scattering coefficient σ_s at the surface for visible light. In fact, the measurements of α performed at Barrow were found to decrease considerably from more than 1.2 to less than 0.7, as σ_s increased gradually from 10 to 50 Mm^{-1}.

[57] As pointed out in sections 2 and 3, great caution is required in interpreting the variations in α from one aerosol class to another, in terms of changes in the shape parameters of the columnar particle size distribution. However, bearing in mind that the relationship between AOD and α is based on the concepts expressed by the Mie theory, exponent α is expected to be very sensitive to the variations in the relative amount of submicron scattering aerosols and, hence, capable of indicating the increase in the vertical content of large accumulation and coarse particles. Therefore parameter α can be very useful in evaluating the intensity of the extinction effects caused by the large and coarse aerosol particle modes or, in cases of cloudy sky measurements, by precipitating crystals.

[58] The analysis of the surface-level sampling measurements of aerosol particles performed by *Hillamo et al.* [1998] at Terra Nova Bay and by *Teinilä et al.* [2000] at Aboa clearly demonstrated that the Antarctic aerosol size distributions are in general multimodal. Since it is well known that columnar aerosol is mainly suspended within the first kilometers of the atmosphere [*Shaw*, 1982], it can be assumed that the number density size distributions of columnar aerosol are more frequently multimodal rather than smoothed (i.e., decreasing gradually as a function of particle diameter throughout the submicron and supermicron size range), as suggested by the *Junge* [1963] model.

[59] Figure 16b shows that the daily mean values of AOD(500 nm) and α determined at the Antarctic coastal sites differ appreciably from those measured at the high plateau stations. The two parameters cover two distinct intervals, since α varied from nearly null values to about 2.0 in the coastal cases, and mainly between 0.5 and more than 2.5 in the high plateau cases, while the AOD values measured at the coastal sites were usually more than twice those observed on the Antarctic Plateau. The volcanic data were found to be widely scattered, since they pertain to the entire decay period of the Pinatubo and Cerro Hudson particles, from their formation in the stratosphere to their vanishing. During this phase of about 2–3 years, AOD tended to decrease slowly and the multimodal size distribution curve of volcanic particles to evolve with time, since the coarse particle modes became gradually more stable with a slight decrease in number concentration, and the submicron modes changed rapidly in both shape and number concentration during the growth period of these particles. However, it is worth noting in Figure 16b that α decreased slowly during the aging period, until gradually clustering around a value close to 0.5, while AOD(500 nm) correspondingly decreased to assume values of around 0.15 during the final evolutionary stage. The high values of α found for relatively low values of AOD(500 nm) can be easily explained, considering that they are given by the sum of two contributions: (1) the former, due to the volcanic particles growing with age and, hence, presenting in general rather low values of α, and (2) the latter, due to the background tropospheric particles, characterized by generally high values of α and lower values of AOD. The plot in Figure 16b also shows that two clusters are formed by the data sets of the thin cirrus clouds and small ice crystals, the latter often raised by the action of strong winds on the iced surfaces that surround the high plateau stations.

[60] Figures 16a and 16b offer an example of how to characterize polar aerosols, showing that Ångström exponent α tends in general to decrease gradually as AOD(500 nm) increases, roughly defining a nonlinear relationship between the two parameters [*Stone*, 2002]. Under pristine conditions, represented for instance by the background Arctic aerosol data and the Antarctic aerosol data taken at the high plateau stations, AOD(500 nm) most frequently has very low values gathered within a very narrow range, these measurements being collected near the lower limit of the Sun photometer sensitivity.

[61] The present characterization of the radiative properties of polar aerosols illustrated by Figures 16a and 16b can be conveniently completed by determining the spectral patterns of real and imaginary parts of the particulate refractive index, for the various Arctic and Antarctic aerosol classes identified in the present study, together with the corresponding spectral curves of single scattering albedo. Table 4 shows the aerosol classes considered for these calculations, together with the average values of AOD(500 nm) and exponent α determined for each class by examining (1) the data sets shown in Figures 5, 6, 8, 9 and 16a for the Arctic aerosols; (2) those presented in Figures 12–14 and 16b for the Antarctic aerosols; and (3) the evaluations of the median values of these parameters given in Table 3. The following procedure was then followed to determine the radiative parameters, consisting of three steps:

[62] 1. The particle size distribution curves were assumed to be monomodal in all cases with $\alpha > 1.25$ (i.e., in models 1 and 8–11 in Table 4) and bimodal for the other seven cases, with $\alpha \leq 1.25$. In the latter, the first mode contains predominantly fine and small accumulation particles, and the second consists mainly of large accumulation and coarse particles. To define these size distribution curves, the lognormal curves of the 6S radiative transfer code [*Vermote et al.*, 1997a, 1997b] were used, with mode diameters equal to 0.01 or 0.02 μm in the first mode and equal to 0.60 or 1.00 μm in the large/coarse particle mode, the choice of the mode diameters being limited by the low number of subroutine

Table 4. Median Values of Ångström Exponent α, Pairs of Mode Diameters and Composition Mass Percentages of the 6S Components Assumed to Define the Particle Size Distribution Curves, the Number Density Concentrations of the Monomodal Particles and the Radiative Properties of Eight Bimodal and Five Monomodal Polar Aerosol Extinction Models, Determined Using the 6S Code Subroutines [*Vermote et al*, 1997a, 1997b]

Model Number	Aerosol Extinction Model	AOD(500 nm)	Ångström Exponent α	Mode Diameter, μm	Mass Percentages of the 6S Code Components			
					Water-Soluble	Oceanic	Dust-Like	Soot
1	background Arctic aerosol	0.015	1.40	0.01	39.0	30.0	30.0	1.0
2	Arctic dense aerosol	0.080	1.00	0.01 and 0.60	35.0, 5.0	10.0, 95.0	54.0, –	1.0, –
3	Arctic haze	0.150	1.25	0.01 and 0.60	65.5	30.0	3.0	1.5
4	Asian dust	0.200	0.80	0.01 and 1.00	24.0, 6.0	10.0, 4.0	66.0, 90.0	–, –
5	boreal smoke	0.300	1.20	0.01 and 0.60	30.0, 29.0	29.0, 35.0	35.0, 35.0	6.0, 1.0
6	Antarctic coastal aerosol (Terra Nova Bay)	0.040	1.00	0.01 and 0.60	79.0, 83.0	19.0, 13.0	1.9, 3.9	0.1, 0.1
7	Antarctic coastal aerosol (Neumayer)	0.060	0.60	0.01 and 0.60	50.5	48.0	2.4	0.1
8	Antarctic inland aerosol (Aboa)	0.050	1.70	0.01	92.0	6.0	1.8	0.2
9	Antarctic high plateau aerosol (Kohnen)	0.015	1.65	0.01	88.0	7.0	4.5	0.5
10	Antarctic high plateau aerosol at Dome C	0.020	1.60	0.01	70.0	30.0	–	–
11	Antarctic high plateau aerosol (OPAC code)	0.015	1.70	0.01	91.0 (sulfates only)	4.5	4.5	–
12	aged volcanic aerosols	0.250	0.50	0.02 and 1.00	with 75% sulfuric acid and 25% liquid water in both modes	with 75% sulfuric acid and 25% liquid water in both modes	with 75% sulfuric acid and 25% liquid water in both modes	with 75% sulfuric acid and 25% liquid water in both modes

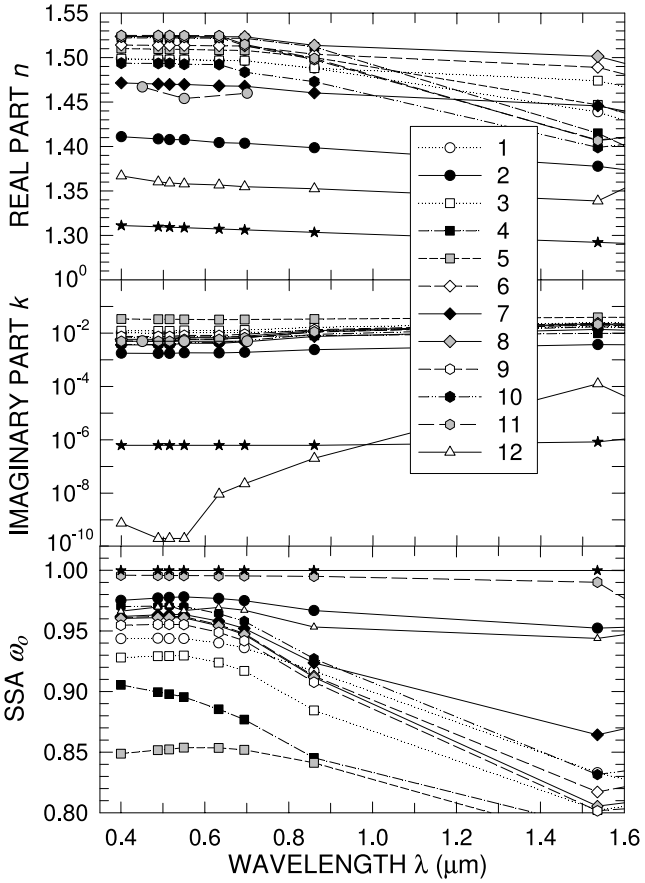

Figure 17. Spectral curves of the real part $n(\lambda)$ and imaginary part $k(\lambda)$ of the particulate refractive index, and single scattering albedo $\omega_o(\lambda)$ for the 12 Arctic and Antarctic aerosol extinction models defined in Table 4. The results obtained for these models are compared with those found for the thin cirrus cloud model (solid stars) and with the spectral values of $n(\lambda)$ determined by *Virkkula et al.* [2006b] at Aboa, excluding the nucleation episodes, for a null value of k (shaded circles) (the relative standard deviations varying between 2.7% and 4.3%). As can be seen, the Aboa measurements agree closely with those of the Antarctic coastal aerosol observed at Neumayer (model 7 in Table 4).

configurations available in the 6S code (as stated by the WPC 112 in the work by *World Meteorological Organization* (*WMO*) [1983]).

[63] 2. The chemical composition characteristics of the 11 aerosol models in Table 4 were defined, taking into account the results obtained at different Arctic and Antarctic sites, described in subsections 3.3 and 3.4. Using the 6S aerosol subroutines describing the four basic aerosol components defined by *WMO* [1983], the mass percentages given in Table 4 were determined for the four 6S components. The Arctic aerosol models were based on the Barrow and Ny Ålesund/Zeppelin results described in the present paper, and the Antarctic aerosol types were characterized separately for the various sites, taking into account the chemical composition mass fractions found at Terra Nova Bay, Neumayer, Halley, Aboa, and Kohnen (models 6–9 in Table 4). The composition of model 10 relative to Dome C was assumed according to the *Six et al.* [2004] results, defining a mix of 70% sulfate and 30% sea salt. Model 11 relative to high plateau sites was determined on the basis of the OPAC code assumptions [*Hess et al.*, 1998], with mass fractions of 91% sulfate, 4.5% sea salt, and 4.5% mineral dust. In addition, the aged volcanic aerosol model was defined in Table 4, relative to both Arctic and Antarctic regions (model 12), based on a bimodal size distribution curve defined in accordance with the results found by *Stone et al.* [1993] and *Pueschel et al.* [1993]. The volcanic particles were assumed to consist of 75% sulphuric acid and 25% liquid water [*Rosen and Hofmann*, 1986], with spectral values of the complex refractive index given by *Palmer and Williams* [1975] and *Irvine and Pollack* [1968], respectively. A thin cirrus cloud model was also defined, represented using a wide lognormal curve of large ice crystals and the ice refractive index data given by *Irvine and Pollack* [1968] to calculate the values of single scattering albedo.

[64] 3. Once the radiative properties of the various modes were established, the number density concentrations were determined only for the bimodal models, by varying in each case the number concentrations of the two modes until fitting the value of parameter α established in Table 4.

[65] The spectral curves of $n(\lambda)$, $k(\lambda)$ and $\omega_o(\lambda)$ determined for the 12 models given in Table 4 are presented in Figure 17, where they are also compared with those determined for the above cirrus cloud model, and the values of $n(\lambda)$ measured by *Virkkula et al.* [2006b] at Aboa, excluding some nucleation episodes. The latter turn out to be lower than all the Antarctic coastal and high plateau aerosol models defined in Table 4, as can be seen in Figure 17. The evaluations of $n(\lambda)$ were found to range from values close to 1.30 (cirrus clouds) to values higher than 1.52 (Antarctic inland and high plateau aerosols, models 8 and 11), while the imaginary part assumes (1) very low values for model 12 (aged volcanic aerosols) and thin cirrus clouds; (2) higher values, ranging from 10^{-3} to 10^{-2}, for the majority of the Arctic and Antarctic aerosol models; and (3) values higher than 10^{-2} for models 3 (Arctic haze) and 5 (boreal smoke). Consequently, $\omega_o(\lambda)$ was found to assume values close to unity for the thin cirrus clouds and model 11 (Antarctic high plateau, OPAC). The values of ω_o found for model 11 do not agree with the estimates performed by *Bodhaine* [1995], who found values of ω_o varying between 0.94 and 0.99 during the austral summer. This is probably due to the fact that the OPAC code totally neglects the presence of soot substances in the Antarctic aerosols, in contradiction with the *Bodhaine* [1995] findings, yielding values of ω_o varying between 0.94 and 0.99. It is sufficient, however, to assume mass fractions of 0.5 and 1% soot substances in the OPAC model, in accordance with the *Wolff and Cachier* [1998] estimates, to obtain values of ω_o of about 0.95 and 0.98, which fit the *Bodhaine* [1995] data very well.

[66] Values of ω_o ranging mainly between 0.93 and 0.98 were obtained at visible wavelengths for the majority of the 12 Arctic and Antarctic aerosol models presented in Figure 17, except for the Asian dust showing values of ~0.90 and the boreal smoke yielding values of about 0.85. The values relative to the Asian dust (model 4) were obtained assuming a null mass fraction of soot particles.

Assuming the presence of a background content of soot particles, with a mass fraction of 1%, values of ω_o varying from 0.88 to 0.85 were obtained at the visible wavelengths, showing that the choice of the absorbing substance mass fractions within a few percents is crucial for determining the single scattering albedo characteristics. However, the values of ω_o, found for two values of k equal to null and 7 10^{-3} in the visible, turn out to be both consistent with the evaluations achieved by *Höller et al.* [2003] during the ACE-Asia experiment, who defined a very wide range of this quantity, from 0.65 to 0.95, for Asian dust transported toward Japan. The present values of ω_o obtained for boreal smoke (model 5) are not too low, if one considers that they contain in general relevant percentages of absorbing particles.

[67] The results shown in Figure 17 can be useful for calculating the direct aerosol radiative forcing at the surface and at the top of the atmosphere (TOA). As pointed out in subsection 2.4, evaluations of instantaneous DARF at the surface occurring during particular episodes of Arctic aerosol transport are suitable for determining the relevant effects of polar aerosols on the Earth's climate, which have been almost completely neglected in the past. Evaluations of the direct aerosol-induced radiative forcing $\Delta F\uparrow$ at TOA can be correctly evaluated using the present results: on the basis of AOD and α measurements carried out at Terra Nova Bay from 1987/1988 to 1993/1994, and of the multimodal chemical composition results found by *Hillamo et al.* [1998], *Cacciari et al.* [2000] calculated the instantaneous values of $\Delta F\uparrow$ at TOA as a function of the solar zenith angle θ_s, using the different isotropic surface reflectance models derived by *Lupi et al.* [2001] from spectral measurements of surface short-wave reflectance performed at various Antarctic sites. For values of AOD(500 nm) ranging mainly between 0.03 and 0.07, the change $\Delta F\uparrow$ in the upwelling flux of short-wave radiation at TOA was mainly estimated to vary (1) between -1 and -3 W m^{-2} in cases where the surface albedo is lower than 0.3 (sea and snow-free land areas) and (2) between +0.7 and +1.7 W m^{-2} in cases where surface albedo is higher than 0.7 (over the inland areas of Antarctica). These evaluations furnished estimates of the forcing efficiency varying from -20 to -35 W m^{-2} for surface albedo equal to 0.30, and from +20 to +50 W m^{-2} for surface albedo equal to 0.7, indicating that the same columnar aerosol loading can induce cooling effects over the oceans and atmospheric warming effects over the continent.

[68] However, more accurate evaluations of both DARF at the surface and $\Delta F\uparrow$ at TOA are required in the polar regions, based on (1) precise measurements of the aerosol radiative properties examined in the present paper and (2) realistic models of anisotropic reflectance from the polar surfaces, appropriately represented in terms of Bidirectional Reflectance Distribution Function (BRDF) models [*Ricchiazzi et al.*, 2005]. On both these aspects, great benefit could be obtained from satellite observations, useful also for validating the calculations of the radiative aerosol-induced forcing effects and the field measurements of the columnar aerosol radiative parameters. Moreover, satellite observations could contribute to achieving more extensive monitoring in space of the spectral values of AOD and α, which are routinely measured at only a few Sun photometer stations in the polar regions. In fact, values of AOD can be retrieved from satellite data within the visible and near-IR channels (like those of MODIS/Terra and Aqua) also in some polar areas. Thus a continuous and systematic validation of the satellite data could be performed through regular comparisons of these retrieved values of AOD with the ground-level measurements of AOD taken at some remote sites. Realistic evaluations of parameter α can be obtained from the satellite images furnished by sensors such as ATSR-2 mounted on board ESA's ERS-2 spacecraft [*Robles González et al.*, 2003], which could be compared with the measurements of α performed at some Sun photometer stations in the Arctic and Antarctica, following some standard procedures in analyzing the spectral data of AOD. In addition, direct measurements of short-wave, long-wave and window radiative upwelling fluxes derived from satellite observation taken by sensors such as CERES mounted aboard the Terra, Aqua and TRMM missions, could be usefully employed to verify the reliability of the TOA radiative forcing calculations provided by radiative transfer models.

[69] Thus nadir observations of polar orbiting imaging spectral radiometers in the visible and near-IR wavelength range are suitable for use in determining the spectral characteristics of AOD. Two different techniques could contribute to aerosol monitoring: (1) single view nadir scans over open water regions, as obtained by instruments like MODIS, MERIS, and SeaWiFS, and (2) dual- (or multi) view observations over snow and ice, as made by MISR, AATSR, and ATSR-2. The generally low values of AOD observed in the polar regions require an improvement in the accuracy of the retrieval methods. Therefore both approaches need to be adapted to polar regions, because the standard procedures do not consider the specifics of polar conditions: spherical atmosphere, refraction, Arctic vertical profile conditions, mostly non-Lambert surface conditions, and many other atmospheric transparency parameters, like those relative to Rayleigh scattering and gaseous absorption.

5. Conclusions

[70] The present comparison between Arctic and Antarctic data offers evidence of the considerable differences characterizing the radiative properties of the respective aerosols. It is true that for polar clean air, columnar aerosols in both regions consist of a mix of very small particles, mainly of marine origins. However, very different columnar loadings and chemical composition characteristics were found more generally in the two polar areas. About 90% of the world's industry is in the Northern Hemisphere, much of it at relatively high (50–60°N) latitude and the atmospheric turbidity conditions are frequently subject in winter and spring to strong changes due to haze and dust transport episodes [*Shaw*, 1982]. Thus the Arctic is not the pristine region it is often thought to be, the sudden variations in the atmospheric turbidity characteristics causing considerable perturbations on the radiation balance of the atmosphere over regional scales. Coastal and high plateau aerosols in Antarctica are quite different in amount and chemical composition, since coastal aerosols are strongly influenced by marine aerosols, while continental aerosols are only weakly and episodically influenced by loadings of sea salt

particles, containing a predominant fraction of small-size aerosols, whose presence is favored by subsidence processes from the free troposphere.

[71] The direct radiative impact of polar aerosols at the surface and at TOA need to be studied more closely through both theoretical studies on the aerosol radiative properties and measurements of the surface reflectance characteristics. The verification of the theoretical results requires the continuous monitoring of aerosol optical properties in conjunction with surface radiation budget measurements. In particular, aerosol properties obtained from in situ measurements should be compared with those provided by Sun radiometers along the Sun path and photometer techniques at the surface, and the two techniques could be combined to integrate the radiative effects of aerosols along the entire atmospheric column. Multispectral AOD measurements, such as those planned by the POLAR-AOD IPY program will provide a valid contribution in developing such verification activities.

[72] The large differences in AOD observed in polar records highlight the importance of assimilating analogous data from other sites to better characterize aerosols spatially and temporally. Figures 16a and 16b illustrate the potential value of assimilating data from various sites to provide an indication of how aerosols differ from pole to pole and, in the case of Antarctica, from coastal sites to the high plateau stations. Using ancillary data, primary trajectory analyses [*Harris and Kahl*, 1994], source regions of different aerosols can be identified and different species can be classified according to their spectral signatures. In order to investigate more thoroughly the radiative effects induced by columnar aerosol polydispersions of different origins on the radiation balance of the polar surface-atmosphere system, the POLAR-AOD IPY Programme plans to achieve more homogeneous evaluations of the AOD spectral series and the related radiative and chemical composition parameters of Arctic and Antarctic aerosols. For this purpose, advantage will be gained from the multiannual experience of the POLAR-AOD groups and the availability of advanced instruments with which long-time series of measurements have been and will be performed at the network stations in both polar regions.

[73] Exploiting the expertise and the potentialities of the various POLAR-AOD groups, the objectives of this IPY program will be pursued through the various activities planned during the International Polar Year.

[74] 1. Deploying advanced Sun and star radiometers to attain a more extensive monitoring of AOD, also by opening new Sun photometer and radiometer stations, such as Eureka (80°00′N, 85°49′E, 10 m MSL) in Northern Canada, Tiksi (71°35′N, 128°47′E, 40 m MSL) in North Central Siberia (Russia) in the Arctic region, Machu Picchu (Peru, 62°05′S, 58°28′W, 10 m MSL) in the Antarctic Peninsula and Maitri (India, 70°46′S, 11°44′E, 132 m MSL) along the coast of the Haakon VII Sea.

[75] 2. Performance of regular calibration campaigns for a rigorous intercomparison among the various Sun photometers employed by the POLAR-AOD groups, to obtain more homogeneous evaluations of the total atmospheric optical depth at various wavelengths. A first workshop was held at Ny Ålesund in early spring 2006, providing preliminary results [*Shiobara et al.*, 2006] and offering the opportunity of checking the accuracy of the AOD measurements given by all the Sun photometers of the POLAR-AOD network. The accuracy performances were estimated to be of ~0.01 at the 500 nm wavelength for the majority of the Sun photometers [*Shiobara et al.*, 2006] and, hence, to satisfy the WMO requirements.

[76] 3. Defining more precise spectral values of Rayleigh scattering optical depth, calculated at the various visible and near-IR wavelengths, for the thermal and moisture conditions normally observed in the polar atmosphere, and using these improved evaluations to correct the total atmospheric optical depth and determine the spectral values of AOD.

[77] 4. Determining realistic absorption models used together with routine measurements and model evaluations of the columnar contents of ozone, nitrogen dioxide, oxygen dimer and water vapor, to correct the spectral measurements of the total atmospheric optical depth for absorption effects.

[78] 5. Adopting consistent procedures to achieve homogeneous calculations of the Ångström turbidity parameters.

[79] 6. Improvement of the aureole sky radiometer techniques for the determination of the sky brightness in almucantar, leading to more reliable evaluations of the real and imaginary parts of the particulate refractive index of columnar aerosol and the other radiative parameters (phase function and asymmetry factor).

[80] 7. Determining more realistic models of anisotropic surface reflectance to represent the different surface albedo characteristics of sea and land polar regions, such as those defined by *Ricchiazzi et al.* [2005] in terms of BRDF models.

[81] 8. Defining appropriate radiative transfer models to calculate the direct radiative forcing induced by polar aerosols at the surface (DARF) and at the top of the atmosphere (TOA) for different BRDF representations of surface reflectance in polar areas.

[82] 9. Analyzing satellite images to achieve a better spatial and temporal coverage of the polar regions, through the retrieval of aerosol parameters and their validation through the ground-based measurements performed at the POLAR-AOD stations, thus attaining a more complete picture of the aerosol radiative properties and the direct aerosol-induced forcing effects at TOA.

[83] 10. Development of systematic in situ measurements of the physical and radiative aerosol parameters, for a better assimilation of the aerosol composition data at the various sites and a more complete characterization of the polar aerosols on the spatial and temporal scales.

[84] **Acknowledgments.** This research was supported by the Programma Nazionale di Ricerche in Antartide (PNRA) and developed as a part of Subproject 2006/6.01: "POLAR-AOD: a network to characterize the means, variability and trends of the climate-forcing properties of aerosols in polar regions." The authors acknowledge NOAA/GMD for the availability of the multiannual series of Barrow and South Pole data from the NOAA/GMD data archives. GOA-UVA thanks the Spanish CICyT for supporting project CGL2006-26188-E/CLI and the EU for funding various proposals (the ALOMAR ARI and eARI (Enhanced Access to Research Infrastructure) Projects and the EU's 5th and 6th Framework Programme (RITA-CT-2003-506208)).

References

Aaltonen, V., H. Lihavainen, V.-M. Kerminen, M. Ginzburg, M. Kulmala, and Y. Viisanen (2006a), Three years of AOD measurements at three bipolar sites, in *NOSA 2006 Aerosol Symposium, Combined With the X Finnish National Aerosol Symposium, Finnish-Czech Aerosol Symposium, and BACCI Workshop*, *Rep. Ser. in Aerosol Sci.*, *83*, edited by H. Vehkamäki et al., pp. 17–20, Finn. Assoc. for Aerosol Res., Helsinki.

Aaltonen, V., H. Lihavainen, V.-M. Kerminen, M. Komppula, J. Hatakka, K. Eneroth, M. Kulmala, and Y. Viisanen (2006b), Measurements of optical properties of atmospheric aerosols in Northern Finland, *Atmos. Chem. Phys.*, *6*, 1155–1164.

Ångström, A. (1964), The parameters of atmospheric turbidity, *Tellus*, *16*, 64–75.

Aoki, K., and Y. Fujiyoshi (2003), Sky radiometer measurements of aerosol optical properties over Sapporo, Japan, *J. Meteorol. Soc. Jpn.*, *81*, 493–513.

Barrie, L. A. (1986), Arctic air pollution: An overview of current knowledge, *Atmos. Environ.*, *20*, 643–663.

Bergin, M. H., E. Meyerson, J. E. Dibb, and P. Mayewski (1998), Comparison of continuous aerosol measurements and ice core chemistry over a 10-year period at South Pole, *Geophys. Res. Lett.*, *25*, 1189–1192.

Bigg, E. K. (1980), Comparison of aerosol at four baseline atmospheric monitoring stations, *J. Appl. Meteorol.*, *19*, 521–533.

Bodhaine, B. A. (1989), Barrow surface aerosol: 1976–1987, *Atmos. Environ.*, *23*, 2357–2369.

Bodhaine, B. A. (1992), The U. S. aerosol monitoring program in Antarctica, *SIF Conf. Proc.*, *35*, 15–25.

Bodhaine, B. A. (1995), Aerosol absorption measurements at Barrow, Mauna Loa and South Pole, *J. Geophys. Res.*, *100*, 8967–8975.

Bodhaine, B. A. (1996), Central Antarctica: Atmospheric chemical composition and atmospheric transport, in *Chemical Exchange Between the Atmosphere and Polar Snow*, *NATO ASI Ser. I*, vol. 43, edited by E. W. Wolff and R. C. Bales, pp. 145–172, Springer, Berlin.

Bodhaine, B. A., and E. G. Dutton (1993), A long term decrease in arctic haze at Barrow, Alaska, *Geophys. Res. Lett.*, *20*, 947–950.

Bory, A. J.-M., P. E. Biscaye, and F. E. Grousset (2003), Two distinct seasonal Asian source regions for mineral dust deposited in Greenland (NorthGRIP), *Geophys. Res. Lett.*, *30*(4), 1167, doi:10.1029/2002GL016446.

Bush, B. C., and F. P. J. Valero (2002), Spectral aerosol radiative forcing at the surface during the Indian Ocean Experiment (INDOEX), *J. Geophys. Res.*, *107*(D19), 8003, doi:10.1029/2000JD000020.

Cacciari, A., C. Tomasi, A. Lupi, V. Vitale, and S. Marani (2000), Radiative forcing effects by aerosol particles in Antarctica, *SIF Conf. Proc.*, *69*, 455–467.

Charlson, R. J., S. E. Schwartz, J. M. Hales, R. D. Cess, J. A. Coakley Jr., J. E. Hansen, and D. J. Hofmann (1992), Climate forcing by anthropogenic aerosols, *Science*, *255*, 423–430.

Chylek, P., and J. A. Coakley Jr. (1974), Aerosols and climate, *Science*, *183*, 75–77.

Damoah, R., N. Spichtinger, C. Forster, P. James, I. Mattis, U. Wandinger, S. Beirle, T. Wagner, and A. Stohl (2004), Around the world in 17 days—Hemispheric-scale transport of forest fire smoke from Russia in May 2003, *Atmos. Chem. Phys.*, *4*, 1311–1321.

de la Mare, W. K. (1997), Abrupt mid-twentieth century decline in Antarctic sea-ice extent from whaling records, *Nature*, *389*, 57–60.

Delene, D. J., and J. A. Ogren (2002), Variability of aerosol optical properties at four North American surface monitoring sites, *J. Atmos. Sci.*, *59*, 1135–1150.

de Mora, S. J., D. J. Wylie, and A. L. Dick (1997), Methanesulphonate and non-sea salt sulphate in aerosol, snow, and ice on the East Antarctic plateau, *Antarct. Sci.*, *9*, 46–55.

De Santis, L. V., C. Tomasi, and V. Vitale (1994), Characterization of Ångström's turbidity parameters in the Po Valley area for summer conditions of the atmosphere, *Nuovo Cimento*, *17C*, 407–430.

Di Carmine, C., M. Campanelli, T. Nakajima, C. Tomasi, and V. Vitale (2005), Retrievals of Antarctic aerosol characteristics using a Sun-sky radiometer during the 2001–2002 austral summer campaign, *J. Geophys. Res.*, *110*, D13202, doi:10.1029/2004JD005280.

Dutton, E. G., and J. R. Christy (1992), Solar radiative forcing at selected locations and evidence for global lower tropospheric cooling following the eruptions of El Chichon and Pinatubo, *Geophys. Res. Lett.*, *19*, 2313–2316.

Dutton, E., G. Anderson, G. Carbaugh, D. Jackson, D. Longenecker, D. Nelson, M. O'Neill, R. Stone, J. Treadwell, and J. Wendell (2004), Solar and thermal atmospheric radiation, in *CMDL Summary Rep.*, *27*, pp. 76–96, Global Monit. Div., Earth Syst. Res. Lab., NOAA, Boulder, Colo.

Forster, C., et al. (2001), Transport of boreal forest fire emissions from Canada to Europe, *J. Geophys. Res.*, *106*, 22,887–22,906.

Gernandt, H., A. Herber, A. P. von der Gathen, M. Rex, A. Rinke, S. Wessel, and S. Kaneto (1996), Variability of ozone and aerosols in the polar atmosphere, *Mem. Natl. Polar Res., Spec. Iss.*, *51*, 189–215.

Hand, J. L., S. M. Kreidenweis, J. Slusser, and G. Scott (2004), Comparisons of aerosol optical properties derived from sun photometry to estimates inferred from surface measurements in Big Bend National Park, Texas, *Atmos. Environ.*, *38*, 6813–6821.

Hänel, G., and K. Bullrich (1978), Physico-chemical property models of tropospheric aerosol particles, *Beitr. Phys. Atmos.*, *51*, 129–138.

Hara, K., K. Osada, M. Kido, M. Hayashi, K. Matsunaga, Y. Iwasaka, T. Yamanouchi, G. Hashida, and T. Fukatsu (2004), Chemistry of sea-salt particles and inorganic halogen species in Antarctic regions: Compositional differences between coastal and inland stations, *J. Geophys. Res.*, *109*, D20208, doi:10.1029/2004JD004713.

Hara, K., K. Osada, M. Kido, K. Matsunaga, Y. Iwasaka, G. Hashida, and T. Yamanouchi (2005), Variations of constituents of individual sea-salt particles at Syowa station, Antarctica, *Tellus, Ser. B*, *57*, 230–246.

Harris, J. M., and J. D. W. Kahl (1994), Analysis of 10-day isentropic flow patterns for Barrow, Alaska: 1985–1992, *J. Geophys. Res.*, *99*, 25,845–25,859.

Herber, A., L. W. Thomason, V. F. Radionov, and U. Leiterer (1993), Comparison of trends in the tropospheric and stratospheric aerosol optical depths in the Antarctic, *J. Geophys. Res.*, *98*, 18,441–18,447.

Herber, A., L. W. Thomason, K. Dethloff, P. Viterbo, V. F. Radionov, and U. Leiterer (1996), Volcanic perturbation of the atmosphere in both polar regions: 1991–1994, *J. Geophys. Res.*, *101*, 3921–3928.

Herber, A., L. W. Thomason, H. Gernandt, U. Leiterer, D. Nagel, K. Schulz, J. Kaptur, T. Albrecht, and J. Notholt (2002), Continuous day and night aerosol optical depth observations in the Arctic between 1991 and 1999, *J. Geophys. Res.*, *107*(D10), 4097, doi:10.1029/2001JD000536.

Hess, M., P. Koepke, and I. Schult (1998), Optical properties of aerosols and clouds: The software package OPAC, *Bull. Am. Meteorol. Soc.*, *79*, 831–844.

Hillamo, R., I. Allegrini, R. Sparapani, and V.-M. Kerminen (1998), Mass size distributions and precursors gas concentrations of major inorganic ions in Antarctic aerosol, *Int. J. Environ. Anal. Chem.*, *71*, 353–372.

Hogan, A. W., S. Barnard, and J. Bortiniak (1979), Physical properties of the aerosol at the South Pole, *Geophys. Res. Lett.*, *6*, 845–848.

Holben, B. N., et al. (1998), AERONET—A federated instrument network and data archive for aerosol characterization, *Remote Sens. Environ.*, *66*(1), 1–16.

Holland, M. M., C. M. Bitz, and B. Temblay (2006), Future abrupt reductions in the summer Arctic sea ice, *Geophys. Res. Lett.*, *33*, L23503, doi:10.1029/2006GL028024.

Höller, R., K. Ito, S. Tohno, and M. Kasahara (2003), Wavelength-dependent aerosol single-scattering-albedo: Measurements and model calculations for a coastal site near the Sea of Japan during ACE-Asia, *J. Geophys. Res.*, *108*(D23), 8648, doi:10.1029/2002JD003250.

Hu, R.-M., E. Gerard, J.-P. and Blanchet (2004), Radiative and climate effects of aerosols over the Arctic, in *Proceedings of the International Symposium on Climate Change*, *WMO/TD-1172*, pp. 124–127, World Meteorol. Organ., Geneva, Switzerland.

Irvine, W. M., and J. B. Pollack (1968), Infrared optical properties of water and ice spheres, *Icarus*, *8*, 324–360.

Jaffe, D., T. Iversen, and G. E. Shaw (1995), Comment on "A long term decrease in arctic haze at Barrow, Alaska" by B. A. Bodhaine and E. G. Dutton, *Geophys. Res. Lett.*, *22*, 739–740.

Japan Meteorological Agency (2006), Antarctic Meteorological Data [CD-ROM], *45*, Tokyo.

Junge, C. E. (1963), *Air Chemistry and Radioactivity*, pp. 111–208, Academic Press, New York.

Kerminen, V.-M., K. Teinilä, and R. Hillamo (2000), Chemistry of sea-salt particles in the summer Antarctic atmosphere, *Atmos. Environ.*, *34*, 2817–2825.

Key, J. R., T. Uttal, R. Stone, X. Wang, S. Frisch, and M. Shupe (2006), SEARCH Atmospheric Element 1: Retrospective analysis of Arctic clouds and radiation from surface and satellite measurements, final report to the NOAA for funding under the SEARCH program, 27 pp., Natl. Environ. Satell., Data, and Inf. Serv., NOAA, Madison, Wis. (Available at http://www.arctic.noaa.gov/aro/reports/fy2005-2006/key-analyis-clouds-element1.doc)

King, M. D. (1982), Sensitivity of constrained linear inversions to the selection of the Lagrange multiplier, *J. Atmos. Sci.*, *39*, 1356–1369.

King, M. D., D. M. Byrne, B. M. Herman, and J. A. Reagan (1978), Aerosol size distributions obtained by inversion of spectral optical depth measurements, *J. Atmos. Sci.*, *35*, 2153–2167.

Koponen, I. K., A. Virkkula, R. Hillamo, V.-M. Kerminen, and M. Kulmala (2003), Number size distributions and concentrations of the continental summer aerosols in Queen Maud Land, Antarctica, *J. Geophys. Res.*, *108*(D18), 4587, doi:10.1029/2003JD003614.

Kuhn, M. N. (1972), Die spektrale Transparenz der Antarktischen Atmosphäre, *Arch. Meteorol. Geophys. Bioklimat., Ser. B*, *20*, 299–344.

Lilijequist, G. H. (1957), *Energy Exchange of an Antarctic Snowfield. Short-Wave Radiation. Norwegian-British-Swedish Antarctic Expedition 1949–1952: Scientific Results*, vol. II, part 1A, 109 pp., Norw. Polar Inst., Oslo.

Lupi, A., C. Tomasi, A. Orsini, A. Cacciari, V. Vitale, T. Georgiadis, R. Casacchia, R. Salvatori, and S. Salvi (2001), Spectral curves of surface reflectance in some Antarctic regions, *Nuovo Cimento*, *24C*, 313–327.

Minikin, A., M. Legrand, J. Hall, D. Wagenbach, C. Kleefeld, E. Wolff, E. C. Pasteur, and F. Ducroz (1998), Sulfur-containing species (sulfate and MSA) in coastal Antarctic aerosol and precipitation, *J. Geophys. Res.*, *103*, 10,975–10,990.

Myhre, C. L., K. Stebel, C. Toledano, V. E. Cachorro, A. M. de Frutos, C. Forster, and J. Schaug (2006), Aerosol optical depth in the European Arctic Region, Chapter 5, in *EMEP/CCC-Report 3/2006, Measurements of Particulate Matter: Status Report 2006*, pp. 73–80, Norw. Inst. for Air Res., Kjeller, Norway.

Nagel, D., A. Herber, L. W. Thomason, and U. Leiterer (1998), Vertical distribution of the spectral aerosol optical depth in the Arctic from 1993 to 1996, *J. Geophys. Res.*, *103*, 1857–1870.

Ohno, T. (2005), Aerosol routine observation operated by the Japan Meteorological Agency, in *WMO/GAW Experts Workshop on a Global Surface Based Network for Long Term Observations of Column Aerosol Optical Properties*, *GAW Rep. 162*, *WMO TD 1287*, pp. 70–71, World Meteorol. Organ., Geneva, Switzerland.

Palmer, K. F., and D. Williams (1975), Optical constants of sulfuric acid; Application to the clouds of Venus?, *Appl. Opt.*, *14*, 208–219.

Piel, C. (2004), Variability of chemical and physical parameters of aerosol in the Antarctic troposphere, *Rep. 476/2004*, 147 pp., Alfred Wegener Inst. für Polar- und Meeresforsch., Bremerhaven, Germany.

Pueschel, R. F., S. A. Kinne, P. B. Russell, and K. G. Snetsinger (1993), Effects of the 1991 Pinatubo volcanic eruption on the physical and radiative properties of stratospheric aerosols, in *IRS '92: Current Problems in Atmospheric Radiation, Proceedings of the International Radiation Symposium, Tallinn (Estonia), 3–8 August 1992*, edited by S. Keevallik and O. Kärner, pp. 183–186, A. Deepak, Hampton, Va.

Quinn, P. K., T. L. Miller, T. S. Bates, J. A. Ogren, E. Andrews, and G. E. Shaw (2002), A 3-year record of simultaneously measured aerosol chemical and optical properties at Barrow, Alaska, *J. Geophys. Res.*, *107*(D11), 4130, doi:10.1029/2001JD001248.

Quinn, P., G. Shaw, E. Andrews, E. G. Dutton, T. Ruoho-Airola, and S. L. Gong (2007), Arctic haze: Current trends and knowledge gaps, *Tellus, Ser. B*, *59*, 99–114.

Radionov, V. F. (1994), Variability of aerosol extinction of solar radiation in Antarctica, *Antarct. Sci.*, *6*(3), 419–424.

Radionov, V. F. (2005), Temporal variability of the aerosol optical characteristics of the atmosphere in the Russian Arctic (Historical review), in *WMO/GAW Experts Workshop on a Global Surface Based Network for Long Term Observations of Column Aerosol Optical Properties*, *GAW Rep. 162*, *WMO TD 1287*, pp. 82–85, World Meteorol. Organ., Geneva, Switzerland.

Radionov, V. F., and M. S. Marshunova (1992), Long-term variations in the turbidity of the Arctic atmosphere in Russia, *Atmos. Ocean*, *30*(4), 531–549.

Radionov, V. F., M. S. Marshunova, E. N. Rusina, K. E. Lubo-Lesnichenko, and Yu. E. Pimanova (1994), Atmospheric aerosol turbidity in polar regions (in Russian), *Izv. Atmos. Oceanic Phys.*, *30*, 797–801.

Radionov, V. F., M. V. Lamakin, and A. Herber (2002), Changes in the aerosol optical depth of the Antarctic atmosphere, *Izv. Atmos. Oceanic Phys.*, *38*, 179–183.

Rahn, K. A., R. D. Borys, and G. E. Shaw (1977), The Asian source of Arctic haze bands, *Nature*, *268*, 713–715.

Randles, C. A., L. M. Russell, and V. Ramaswamy (2004), Hygroscopic and optical properties of organic sea salt aerosol and consequences for climate forcing, *Geophys. Res. Lett.*, *31*, L16108, doi:10.1029/2004GL020628.

Ricchiazzi, P., W. O'Hirok, and C. Gautier (2005), The effect of non-Lambertian surface reflectance on aerosol radiative forcing, paper presented at Fifteenth ARM Science Team Meeting, U.S. Dep. of Energy, Daytona Beach, Fla., 14–18 March.

Robinson, D. A. (1997), Hemispheric snow cover and surface albedo for model validation, *Ann. Glaciol.*, *25*, 241–245.

Robles González, C., M. Schaap, G. de Leeuw, P. J. H. Builtjes, and M. van Loon (2003), Spatial variation of aerosol properties over Europe derived from satellite observations and comparison with model calculations, *Atmos. Chem. Phys.*, *3*, 521–533.

Rosen, J. M., and D. J. Hofmann (1986), Optical modeling of stratospheric aerosol: Present status, *Appl. Opt.*, *25*, 410–419.

Russell, P. B., J. M. Livingston, P. Hignett, S. Kinne, J. Wong, A. Chien, R. Bergstrom, P. P. Durkee, and P. V. Hobbs (1999), Aerosol-induced radiative flux changes off the United States mid-Atlantic coast: Comparison of values calculated from sunphotometer and in situ with those measured by airborne pyranometer, *J. Geophys. Res.*, *104*, 2289–2307.

Sakunov, G. G., and N. P. Rusin (1980), Background characteristic of atmospheric transparency regime in the Antarctic (in Russian), in *Studies of Antarctic Climate*, pp. 20–26, Gidrometeoizdat, St. Petersburg, Russia.

Schwartz, S. E., et al. (1995), Group report: Connections between aerosol properties and forcing of climate, in *Aerosol Forcing of Climate*, edited by R. J. Charlson and J. Heintzenberg, pp. 251–280, John Wiley, New York.

Serreze, M. C., J. A. Maslanik, T. A. Scambos, F. Fetterer, J. Stroeve, K. Knowles, C. Fowler, S. Drobot, R. G. Barry, and T. M. Haran (2003), A record minimum arctic ice extent and area in 2002, *Geophys. Res. Lett.*, *30*(3), 1110, doi:10.1029/2002GL016406.

Sharma, S., E. Andrews, L. A. Barrie, J. A. Ogren, and D. Lavoué (2006), Variations and sources of equivalent black carbon in the high Arctic revealed by long-term observations at Alert and Barrow: 1989–2003, *J. Geophys. Res.*, *111*, D14208, doi:10.1029/2005JD006581.

Shaw, G. E. (1982), Atmospheric turbidity in the polar regions, *J. Appl. Meteorol.*, *21*, 1080–1088.

Shaw, G. E. (1983), Evidence of a central Eurasian source area of Arctic haze in Alaska, *Nature*, *299*, 815–818.

Shaw, G. E. (1988), Antarctic aerosols: A review, *Rev. Geophys.*, *26*, 89–112.

Shaw, G. E., J. A. Reagan, and B. H. Herman (1973), Investigations of atmospheric extinction using direct solar radiation measurements made with a multiple wavelength radiometer, *J. Appl. Meteorol.*, *12*, 374–380.

Shiobara, M., M. Tanaka, T. Nakajima, and H. Ogawa (1987), Spectral measurements of direct solar radiation and sky brightness distribution at Syowa Station, Antarctica, in *Atmospheric Radiation—Progress and Prospects, Proceedings of the Beijing International Radiation Symposium*, edited by K.-N. Liou and Z. Xiuji, pp. 629–637, Sci. Press, Beijing.

Shiobara, M., R. Stone, A. Herber, V. Vitale, C. Tomasi, and the Polar AOD Campaign Participants (2006), The first Polar-AOD radiometer inter-comparison experiment at Ny-Ålesund in the Arctic: Preliminary result and validation analysis, paper presented at 29th Symposium on Polar Meteorology and Glaciology, Natl. Inst. for Polar Res., Tokyo, 20–21 Nov.

Six, D., M. Fily, S. Alvain, P. Henry, and J.-P. Benoist (2004), Surface characterization of the Dome Concordia area (Antarctica) as a potential satellite calibration site, using SPOT4/Vegetation instrument, *Remote Sens. Environ.*, *89*, 83–94.

Sokolik, I., A. Andronova, and T. C. Johnson (1993), Complex refractive index of atmospheric dust aerosols, *Atmos. Environ., Part A*, *27*, 2495–2502.

Stohl, A., et al. (2006), Pan-Arctic enhancements of light absorbing aerosol concentrations due to North American boreal forest fires during summer 2004, *J. Geophys. Res.*, *111*, D22214, doi:10.1029/2006JD007216.

Stone, R. S. (1997), Variations in western Arctic temperatures in response to cloud radiative and synoptic-scale influences, *J. Geophys. Res.*, *102*, 21,769–21,776.

Stone, R. S. (2000), Climate monitoring at Barrow, Alaska, and South Pole; An overview of U.S. studies of the polar surface radiation balance and aerosols, *SIF Conf. Proc.*, *69*, 83–98.

Stone, R. S. (2002), Monitoring aerosol optical depth at Barrow, Alaska, and South Pole; Historical overview, recent results and future goals, *SIF Conf. Proc.*, *80*, 123–144.

Stone, R. S., J. Key, and E. Dutton (1993), Properties and decay of stratospheric aerosols in the Arctic following the 1991 eruptions of Mount Pinatubo, *Geophys. Res. Lett.*, *20*, 2359–2362.

Stone, R. S., E. G. Dutton, J. M. Harris, and D. Longenecker (2002), Earlier spring snowmelt in northern Alaska as an indicator of climate change, *J. Geophys. Res.*, *107*(D10), 4089, doi:10.1029/2000JD000286.

Stone, R. S., G. Anderson, E. Andrews, E. Dutton, J. Harris, E. Shettle, and A. Berk (2005), Asian dust signatures at Barrow: observed and simulated, paper presented at IEEE Workshop on Remote Sensing of Atmospheric Aerosol, An Honorary Workshop for Prof. J. A. Reagan, Univ. of Ariz., Tucson, 5–6 April.

Ström, J., J. Umegård, K. Tørseth, P. Tunved, H.-C. Hansson, K. Holmén, V. Wismann, A. Herber, and G. König-Langlo (2003), One year of particle size distribution and aerosol chemical composition measurements at the Zeppelin station, Svalbard, March 2000–March 2001, *Phys. Chem. Earth*, *28*, 1181–1190.

Teinilä, K., V.-M. Kerminen, and R. Hillamo (2000), A study of size-segregated aerosol chemistry in the Antarctic atmosphere, *J. Geophys. Res.*, *105*, 3893–3904.

Toledano, C., V. E. Cachorro, A. Berjón, M. Sorribas, R. Vergaz, Á. M. de Frutos, M. Antón, and M. Gausa (2006), Aerosol optical depth at ALOMAR Observatory (Andøya, Norway) in summer 2002 and 2003, *Tellus, Ser. B*, *58*, 218–228.

Tomasi, C., F. Prodi, M. Sentimenti, and G. Cesari (1983), Multiwavelength sun-photometers for accurate measurements of atmospheric extinction in the visible and near-IR spectral range, *Appl. Opt.*, *22*, 622–630.

Tomasi, C., V. Vitale, and M. Tagliazucca (1989), Atmospheric turbidity measurements at Terra Nova Bay during January and February 1988, *SIF Conf. Proc.*, *20*, 67–77.

Tomasi, C., V. Vitale, and G. Zibordi (1991), Multiwavelength sun-photometric measurements of the atmospheric turbidity parameters at Terra Nova Bay during January 1990, *SIF Conf. Proc.*, *34*, 125–142.

Tomasi, C., S. Marani, V. Vitale, F. Wagner, A. Cacciari, and A. Lupi (2000), Precipitable water evaluations from infrared sun-photometric

measurements analyzed using the atmospheric hygrometry technique, *Tellus, Ser. B*, *52*, 734–749.

Town, M. S., V. P. Walden, and S. G. Warren (2005), Spectral and broadband longwave downwelling radiative fluxes, cloud radiative forcing, and fractional cloud cover over the South Pole, *J. Clim.*, *18*, 4235–4252.

Tunved, P., H.-C. Hansson, V.-M. Kerminen, J. Ström, M. Dal Maso, H. Lihavainen, Y. Viisanen, P. P. Aalto, M. Komppula, and M. Kulmala (2006), High natural aerosol loading over boreal forests, *Science*, *312*, 261–263.

VanCuren, R. A., and T. A. Cahill (2002), Asian aerosols in North America: Frequency and concentration of fine dust, *J. Geophys. Res.*, *107*(D24), 4804, doi:10.1029/2002JD002204.

Vermote, E., D. Tanré, J. L. Deuzé, M. Herman, and J. J. Morcrette (1997a), Second Simulation of the Satellite Signal in the Solar Spectrum (6S), 6S user guide, version 2, Univ. de Lille, France.

Vermote, E., D. Tanré, J. L. Deuzé, M. Herman, and J. J. Morcrette (1997b), Second Simulation of the Satellite Signal in the Solar Spectrum (6S): An overview, *IEEE Trans. Geosci. Remote Sens.*, *35*, 675–685.

Vinnikov, K. Y., A. Robock, R. J. Stouffer, J. E. Walsh, C. L. Parkinson, D. J. Cavalieri, J. F. B. Mitchell, D. Garrett, and V. F. Zakharov (1999), Global warming and Northern Hemisphere sea ice extent, *Science*, *286*, 1934–1937.

Virkkula, A., I. K. Koponen, R. Hillamo, and M. Kulmala (2000), Optical properties and volume concentration of atmospheric aerosol between Europe and Antarctica, *J. Aerosol. Sci.*, *31*, S272–S273.

Virkkula, A., K. Teinilä, R. Hillamo, V.-M. Kerminen, S. Saarikoski, M. Aurela, I. K. Koponen, and M. Kulmala (2006a), Chemical size distributions of boundary layer aerosol over the Atlantic Ocean and at an Antarctic site, *J. Geophys. Res.*, *111*, D05306, doi:10.1029/2004JD004958.

Virkkula, A., I. K. Koponen, K. Teinilä, R. Hillamo, V.-M. Kerminen, and M. Kulmala (2006b), Effective real refractive index of dry aerosols in the Antarctic boundary layer, *Geophys. Res. Lett.*, *33*, L06805, doi:10.1029/2005GL024602.

Vitale, V., and V. F. Radionov (2005), Aerosol optical depth measurements in polar regions, in *WMO/GAW Experts Workshop on a Global Surface Based Network for Long Term Observations of Column Aerosol Optical Properties*, *GAW Rep. 162*, *WMO TD 1287*, pp. 75–81, World Meteorol. Organ., Geneva, Switzerland.

Vitale, V., and C. Tomasi (1990), Atmospheric turbidity measurements at Terra Nova Bay with the multispectral sun-photometer model UVISIR, *SIF Conf. Proc.*, *27*, 89–104.

Wehrli, C. (2005), GAWPFR: A network of Aerosol Optical Depth observations with Precision Filter Radiometers, in *WMO/GAW Experts Workshop on a Global Surface Based Network for Long Term Observations of Column Aerosol Optical Properties*, *GAW Rep. 162*, *WMO TD 1287*, pp. 36–39, World Meteorol. Organ., Geneva, Switzerland.

Wolff, E. W., and H. Cachier (1998), Concentrations and seasonal cycle of black carbon in aerosol at a coastal Antarctic station, *J. Geophys. Res.*, *103*, 11,033–11,041.

World Meteorological Organization (1983), Report of WMO (CAS)/Radiation Commission of IAMAP Meeting of Experts on Aerosols and their Climatic Effects (Williamsburg, Virginia, USA, 28–30 March, 1983), edited by A. Deepak and H. E. Gerber, *Rep. WCP-55*, Geneva.

V. Aaltonen, R. Hillamo, H. Lihavainen, and A. Virkkula, Finnish Meteorological Institute, FIN-00101 Helsinki, Finland.

E. Andrews and R. S. Stone, Global Monitoring Division, NOAA, Boulder, CO 80305, USA.

S. Blindheim, M. Frioud, and M. Gausa, Andoya Rocket Range, N-8483 Andenes, Norway.

V. E. Cachorro, P. Ortiz, and C. Toledano, Departamento de Óptica y Física Aplicada, Facultad de Ciencias, Universidad de Valladolid, E-47071 Valladolid, Spain. (chiqui@baraja.opt.cie.uva.es; jportiz@baraja.opt.cie.uva.es; toledano@baraja.opt.cie.uva.es)

M. Campanelli, Institute of Atmospheric Sciences and Climate, Consiglio Nazionale delle Ricerche, Area della Ricerca, Via Fosso del Cavaliere 100, I-00133 Rome, Italy.

A. M. de Frutos, Grupo de Óptica Atmosférica, Departamento de Óptica y Física Aplicada, Facultad de Ciencias, Universidad de Valladolid, E-47071 Valladolid, Spain. (angel@baraja.opt.cie.uva.es)

C. Di Carmine, A. Lupi, C. Tomasi, and V. Vitale, Institute of Atmospheric Sciences and Climate, Consiglio Nazionale delle Ricerche, Area della Ricerca, Via P. Gobetti 101, I-40129 Bologna, Italy. (c.tomasi@isac.cnr.it)

G. H. Hansen, C. L. Myhre, and K. Stebel, Polar Environmental Centre, Norwegian Institute for Air Research, N-9296 Tromsø, Norway.

A. Herber, Climate System Division, Alfred Wegener Institute for Polar and Marine Research, Building C-106, Am Handelshafen 12, D-27570 Bremerhaven, Germany.

T. Petelski and T. Zielinski, Institute of Oceanology, Polish Academy of Sciences, 81-712 Sopot, Poland.

V. Radionov, Arctic and Antarctic Research Institute, St. Petersburg 199397, Russia.

S. Sharma, Science and Technology Branch, Environment Canada, 4905 Dufferin Street, Toronto, ON, Canada M3H 5T4.

J. Ström, Department of Applied Environmental Science, Stockholm University, SE-10691 Stockholm, Sweden.

R. Treffeisen, Climate System Division/Physical and Chemical Processes in the Atmosphere, Alfred Wegener Institute for Polar and Marine Research, Building A45-207, Telegrafenberg A43, D-14473 Potsdam, Germany.

W. von Hoyningen-Huene, Institute of Environmental Physics/Remote Sensing, University of Bremen, Otto-Hahn-Allee 1, D-28334 Bremen, Germany. (hoyning@iup.physik.uni-bremen.de)

C. Wehrli, Physikalisch-Meteorologisches Observatorium/World Radiation Centre, CH-7260 Davos, Switzerland.

T. Yamanouchi, National Institute of Polar Research, Tokyo 173-8515, Japan.